A mussel-inspired, antibacterial, antioxidant, injectable composite hydrogel for the sustain delivery of salvianolic acid B for the treatment of frozen shoulder

Yan Yan [a],[1], Xinhao Li [a],[1], Chen Chen [b], Dedong Cui [a], Zhuo Wang [a], Ming Li [a], Yi Long [a], Jinming Zhang [a], Cheng Li [a], Zhiling Wang [a], Chuanhai Zhou [a], Zeyu Yao [a], Dan Wang [c], Jingyi Hou [a],[**], Rui Yang [a],[*]

[a] *Department of Orthopedics, Sun Yat-sen Memorial Hospital, Sun Yat-sen University, Guangzhou, 510000, China*
[b] *Department of Geriatric Dentistry, NMPA Key Laboratory for Dental Materials National Engineering Laboratory for Digital and Material Technology of Stomatology, Peking University School and Hospital of Stomatology, Beijing, 100081, China*
[c] *School of Biomedical Science, The Chinese University of Hong Kong, Hong Kong, 999077, China*

ARTICLE INFO

ABSTRACT

Frozen shoulder (FS) manifests as progressively worsening pain and a reduction in shoulder range of motion (ROM). Salvianolic acid B (SaB) is recently expected to be used in the treatment of fibrosis diseases including FS. We firstly demonstrate that SaB can effectively hinder the progression of oxidative stress, inflammation, and pathological fibrosis within the synovial tissue in FS, potentially leading to the reduction or reversal of capsule fibrosis and joint stiffness. For further clinical application, we design and synthesize a novel, superior, antioxidant and antibacterial CSMA-PBA/OD-DA (CPDA) hydrogel for the delivery of SaB. In vitro experiments demonstrate that the CPDA hydrogel exhibits excellent biocompatibility and rheological properties, rendering it suitable for intra-articular injections. Upon injection into the contracted joint cavity of FS model rat, the SaB-CPDA hydrogel accelerate the recovery of ROM and exhibit superior anti-fibrosis effect, presenting the promise for the treatment of FS in vivo.

1. Introduction

Frozen shoulder (FS) manifests as progressively worsening pain and a reduction in shoulder range of motion (ROM) [1,2]. This prevalent issue has an incidence ranging from 2 % to 5 %, with an average acute phase lasting 1–2.5 years [3]. Presently, the primary treatments for FS include exercise, physiotherapy, and intra-articular glucocorticoid injections [4,5]. However, these interventions primarily target symptom relief, lacking a widely acknowledged therapeutic approach addressing the occurrence and progression of the disease. Given the slow onset of benefits from exercise and physiotherapy and the rapid failure and limitations associated with glucocorticoids [6,7], patients often endure prolonged periods of shoulder pain and restricted ROM. Consequently, approximately 40 % of FS patients continue to endure persistent

low-level restrictions and pain beyond the initial acute phase [1,8].

Numerous studies have sought to elucidate the onset of FS, generally recognizing inflammation and pathological fibrosis in the shoulder joint as the primary etiological processes [9–11]. Further hypothesis claimed that inflammation precedes, and even lead to pathologic fibrosis. In 1997, Rodeo et al. demonstrated that persistent stimulation with TGF-β1 and PDGF could induce fibrosis in the shoulder capsule [12]. Subsequent research reported an association between inflammatory cytokines, such as IL-6, IL-8, TNF-α, and M-CSF, and the fibrotic process in FS [13]. Moreover, other studies have shown that the imbalance between MMPs (Matrix Metalloproteinases) and TIMPs (Tissue Inhibitors of Metalloproteinases) directly contributes to the excessive accumulation of extracellular matrix (ECM) in FS (Rodeo et al., 1997; Lubis et al., 2013; Akbar et al., 2019; Dakin et al., 2019) [12,14–16]. Additionally,

Hagiwara et al. performed DNA microarray analysis on tissues from FS patients, revealing elevated gene expression associated with fibrosis, inflammation, and chondrogenesis. This suggests that all three aspects may play a pivotal role in the development of FS [11]. While these studies have inspired researchers to explore the development of FS at the tissue level, they have not adequately explained the cellular changes in the capsular synovium.

Fibroblasts are widely acknowledged as pivotal effector cells in various fibrotic diseases, including FS [17–20]. Akbar et al. demonstrated that activated synovial fibroblasts (SFs) in FS produce elevated levels of inflammatory cytokines, including IL-6, IL-8, and CCL-20, shedding light on the synergistic effects between SF activation and dysregulated inflammatory cytokines [15]. Additionally, IL-17A appeared to trigger profibrotic and inflammatory responses in fibroblasts via the TRAF-6/NF-κB pathway in FS [21]. According to our prior research, IL-6 was also identified as a key inducer of pathological fibrosis in FS [22]. Nevertheless, additional research is required to elucidate the precise link between inflammation and pathological fibrosis in FS, along with its underlying mechanisms.

Salvianolic acid B (SaB) is a small molecule isolated from the root of *Salviae Miltiorrhizae*. Recently, SaB has garnered attention for its potential anti-fibrotic, anti-inflammatory, antioxidant, and anti-apoptotic properties [23]. It has also demonstrated therapeutic effects in various fibrotic diseases, including cirrhosis, lung fibrosis, systemic sclerosis, and hyperplastic scars (Tao et al., 2021; Zhang et al., 2021; Wu et al., 2019; Liu et al., 2021) [24–27]. In a previous study, we were the first to demonstrate that SaB reduces ECM deposition in a rat model of FS [28]. However, systemic administration of SaB is associated with unpredictable side effects and a rapid decline in SaB's blood concentration, making it challenging to sustain adequate drug levels in the shoulder joint over an extended period, particularly within diseased synovial tissue. Traditional drug delivery methods involve mixing drugs directly with sterile gauze or hydrogel, which is straightforward and convenient but comes with numerous limitations [29]. Notably, drugs loaded in this manner are quickly released or absorbed by the gauze, diminishing their biological effectiveness. Consequently, this shortens the duration of drug action, hindering the attainment of long-term sustained efficacy in the affected area.

Hydrogels featuring highly hydrated polymeric networks are excellent delivery systems with sustained-release capabilities for encapsulating small-molecule drugs [30]. Due to the methacrylation of amino and carboxyl groups on the side chains, methacrylated chitosan (CSMA) can undergo rapid photo-crosslinking. Furthermore, it retains the Arg-Gly-Asp (RGD) sequence and enzymatic degradation properties that promote cell adhesion, enhance cell proliferation, and regulate cell viability, thus improving cell-substrate interactions. Therefore, CSMA is commonly used in 3D cell culture to study cell proliferation, migration, differentiation, and tissue engineering [31]. However, pure CSMA hydrogels exhibit poor mechanical properties and relatively fast degradation rates. To address the issue of poor mechanical properties in CSMA hydrogels, we have designed a dual-network hydrogel using a natural, degradable material with antioxidant and antibacterial properties for localized SaB delivery. CSMA-PBA was synthesized through the esterification of CSMA and phenylboronic acid (PBA). OD-DA was synthesized by reacting oxidized dextran (OD) with dopamine (DA). We dissolved CSMA-PBA, OD-DA, and 2959 in water and polymerized them under ultra violet (UV) irradiation to produce the CPDA hydrogel. On the one hand, the natural polysaccharide hydrogel has good biocompatibility and application prospects. On the other hand, the design of the dual network was associated with good mechanical properties and sustain release ability and can achieve better pH response [32,33]. In addition, the introduction of OD-DA endowed the hydrogels with good antioxidant and antimicrobial abilities [34]. In our system, water-soluble SaB is encapsulated within the CPDA hydrogel, releasing slowly over time.

The objective of this study is to develop a novel hydrogel material for local delivery of SaB, with the capability of prolonging its retention time within the shoulder joint through sustained release. This multifunctional system has the capacity to serve a triple role in mitigating pathological fibrosis, inflammation, and oxidative stress. Additionally, we aspire to investigate the underlying mechanism of SaB's impact on SFs and elucidate its therapeutic effects on FS (see Scheme 1).

2. Materials and methods

2.1. Study approval

The current study was approved by the Ethics Committee of the Sun Yat-sen Memorial Hospital of Sun Yat-sen University, Guangzhou, China (permit no: SYSKY-2023-872-01). Full informed consent was obtained from all patients. The sample size for tissue- and cell-based assays were determined based on sample availability and technical needs.

2.2. Patients

Patients with frozen shoulder were diagnosed according to the medical history, physical examination and arthroscopic manifestations. A 3.5 mm grasping biopsy forceps was used to obtain synovial tissue biopsies under arthroscopy. 8 patients with FS were recruited from July 2022 to July 2023 in Sun Yat-sen University consecutively. All patients signed the contract for permission to use their tissue for experimental purposes. Demographics and characteristics of patients are shown in Table 1.

### 2.3. Cell isolation and culture

The biopsied samples were rinsed adequately three times with phosphate buffered saline (PBS; Jetbio, China). Thereafter, the samples were minced finely and digested with 0.2 % type I collagenase (Sigma Aldrich, Germany) in high-glucose Dulbecco's modified Eagle's medium (high-glucose DMEM; Gibco, USA) containing 10 % fetal bovine serum (FBS; Gibco, USA). After incubation of 2 h at 37 °C, cells were collected through centrifugation (1000 rpm, 5 min), washed three times with PBS, and resuspended with high-glucose DMEM containing 10 % FBS. After then, cells were transferred to a T25 culture flask (Jetbio, China) and allowed to attach for 3–5 days. Those non-adherent cells were removed after changing the medium. The medium was changed every 2–3 days. The synovial fibroblasts were passaged when reaching 80–90 % confluence, and those from passage 3–5 were used for subsequent experiments. The identification of synovial fibroblasts was presented in our previous work.

2.4. RNA-seq and analysis

Total mRNA extracted from the synovium fibroblasts was purified and reversely transcribed into cDNA. The amplified cDNA was then sequenced on Illumina Hiseq 6000 platform (Illumina, USA) by LC science (Hangzhou, China), following the vendor's recommended protocols. Genes differential expression analysis was performed by DESeq2 software between two different groups (and by edgeR between two samples). The genes with the parameter of false discovery rate (FDR) below 0.05 and absolute fold change ≥2 were considered differentially expressed genes. Differentially expressed genes were then subjected to enrichment analysis of Gene ontology (GO) functions and Kyoto Encyclopedia of Genes and Genomes (KEGG) pathways.

2.5. In vitro anti-ferroptosis effect of SaB

Western blotting: SFs were lysed using cell lysis buffer (CWBiotech, China) containing Protease inhibitors (1:100; CWBiotech, China) and Phosphatase inhibitors (1:100; CWBiotech, China) and the protein concentrations were quantified with a protein assay kit (Vazyme,
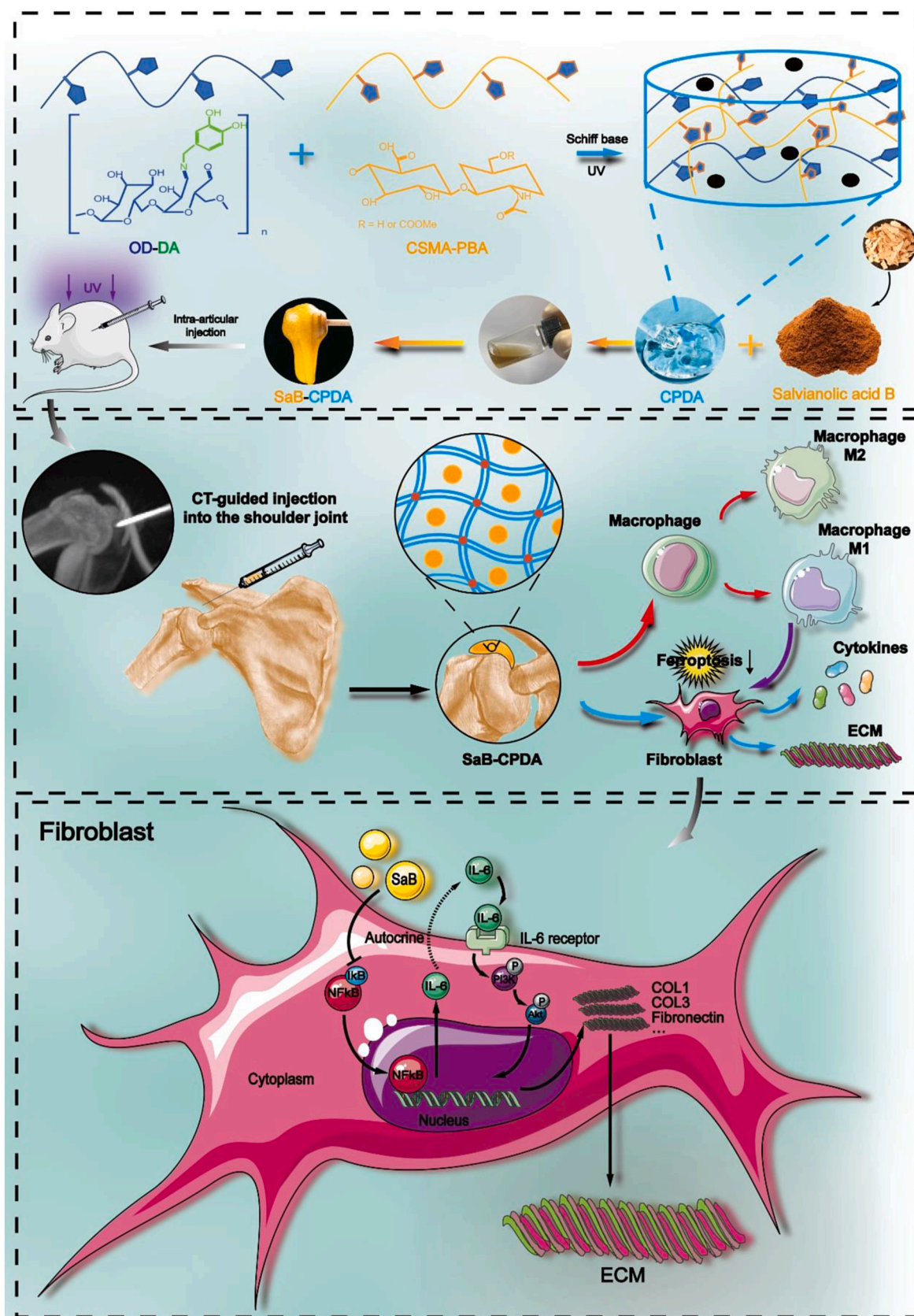
Scheme 1. Scheme illustration for the preparation of CPDA that can delivery and continuously release SaB. Intra-articular injection of SaB-CPDA to achieve the combination of inhibiting inflammation anti-ferroptosis and anti-fibrosis therapeutic effect in FS.

Table 1
Baseline characteristics of FS patients.

Gender	Male	Female	p value
Number	4	4	
Age (years)	48.01	49.25	> 0.05
ROM (passive)			
Flex	83.75 ± 21.36	110.39 ± 18.26	> 0.05
Abd	81.25 ± 8.54	92.51 ± 25.03	> 0.05
ER	25.34 ± 4.08	24.25 ± 5.68	> 0.05
Shoulder function			
ASES	39.25 ± 8.99	43.32 ± 11.34	> 0.05
Constant Murley	34.21 ± 5.45	43.75 ± 11.30	> 0.05
UCLA	15.97 ± 3.37	16.25 ± 3.77	> 0.05

Mean values are expressed as mean ± standard deviation *Statistical significance (a = 0.05).
FS: Frozen shoulder; ROM: range of motion; Flex: flexion; Abd: abduction; ER: external rotation.
ASES: American Shoulder and Elbow Surgeons Scale; UCLA: the university of California at Los Angeles shoulder rating scale.

China). Equal amounts of protein extracts were electro-phoresed on 10 or 12 % gels and then transferred to PVDF membranes (Millipore, USA). The PVDF membranes were blocked with 5 % bovine serum albumin (Biosharp, China) and incubated with primary antibodies. The specific antibody-antigen complexes were detected using an enhanced chemiluminescence kit (Vazyme, China). Band images were captured using the Bio-Rad Gel Doc XR documentation system (Bio-Rad, USA). The expression of Nrf2, SLC7A11 and GPX4 were detected and standardized to GAPDH.

MDA assay: The relative MDA concentration in SFs was assessed by Lipid eroxidation Assay Kit (Abcam). Briefly, the SFs were seeded in 6-well plates at 5×10^4 cells/well for 24 h. Ten the SFs were treated with MDA lysis buffer and reacted with thiobarbituric acid (TBA) to generate an MDA-TBA adduct. The absorbance of the MDA-TBA adduct at 532 nm was detected using an ultraviolet spectrophotometer (Termo Fisher Scientific, USA).

Lipid ROS detection: The lipid ROS was detected using a BODIPY 581/591C11 kit (Thermo Fisher Scientific, USA). The synovial fibroblasts were seeded in 6-well plates at 5×10^4 cells/well for 24 h and treated with SaB, erastin (Selleck, China) and Fer-1 (Selleck, China) for 24 h. Then cells were stained with 2 μM C11-BODIPY (581/591) probe according to the manufacturer's instructions. Synovial fibroblasts were visualized using fluorescence microscopy (Leica, Germany) and analyzed by Image J software (NIH, Bethesda, MD, USA). The oxidized BODIPY (O-BODIPY) were observed at excitation/emission wavelengths of 488/510 (traditional FITC filter set), while the reduced BODIPY (R-BODIPY) were observed at excitation/emission wavelengths of 581/591 nm (Texas Red filter set).

2.6. In vitro effect of SaB on polarization of macrophages and fibrosis

Flowcytometry: The RAW 264.7 (Procell, China) were seeded in 6-well plates at 5×10^4 cells/well for 24 h and treated with IFN-γ (Abclonal, China) + LPS (Abclonal, China), IL-4 (Abclonal, China) or SaB to induce the polarization of macrophages. After 24 h, the cells on the plate were harvested with trypsin and resuspended at 3×10^5/mL for flowcytometry to detect F4/80, CD86 and CD206 expression.

Transwell assay: Polarized RAW 264.7 were seeded into the lower transwell chamber and add 400 μl of complete medium. 24 h later, SFs were seeded at a density of 1.0×10^4 cells in transwell insert with 100 μL of medium without FBS. After 24 h, the upper chamber was removed, and the cells on the sieve at the bottom of the chamber were stained with 0.1 % crystal violet. The morphology of cell was captured by an inverted microscope (Nikon, Japan)

Western blotting: RAW 264.7 was induced to polarize towards different directions according to methods mentioned above. The culture medium was then refreshed and collected after 24 h. Collected medium

was then used in the culture of SFs for 24 h. The expression of COL1, COL3, FN, α-SMA and p65 in SFs were detected using western blotting and standardized to GAPDH.

2.7. In vitro effect of SaB on inflammatory pathways

Western blotting: The expression of COL1, COL3, FN, p65, pp65 and IL-6 were detected using western blotting and standardized to GAPDH.

Enzyme-linked immunosorbent assays (ELISA): After administration of SaB for 48 h, concentrations of IL-6 in SFs culture supernatant were detected using ELISAs kits for IL-6 (R&D Systems, United States) according to the manufacturer's protocol.

Immunofluorescence (IF): Capsule sections from FS group and control group were stained with antibody against IL-6 (Abcam, UK) and pp65 (Abcam, UK). The stained images were recorded by fluorescence microscopy (Zeiss, Germany). SFs were pre-incubated with medium from polarized macrophages and then stained with antibody against p65 (Abcam, UK). The stained images were recorded by confocal microscope (Zeiss, Germany).

Cell transfection: SiRELA, scrambled negative control siRNA, *RELA* overexpression plasmid and negative vector were obtained from Genecreate (Wuhan, China). The final concentration of siRNA was 20 μM, and the final plasmid concentration was 100 μg/μl. SFs were seeded in 6-well plates (1.5×10^5 cells/well) and transfected with siRNA, negative control siRNA, *RELA* overexpression plasmid or negative vector via Lipofectamine 3000 (Thermo Fisher Scientific, USA) according to the manufacturer's instructions. After 48 h, cells were harvested to quantify the mRNA or protein expression.

Quantitative reverse transcription polymerase chain reaction (RT-qPCR): Total RNA of the synovial fibroblasts was isolated using an RNA Purification Kit (EZBioscience, USA) and transcribed into cDNA with a PrimeScript RT reagent kit (EZBioscience, USA). RT-qPCR analyses were then performed using a LightCycler 480 RealTime PCR System (Roche, Basel, Switzerland) with a SYBR Premix Ex Taq (Accurate Biology, China). The results were normalized to the expression level of GAPDH and the relative expression of each gene was determined with the 2^(−ΔΔCt) method. The forward and reverse primers for each gene are listed in Table 2.

Luciferase assay: SFs were seeded into 96-well plates at a density of 5×10^3 cells per well and transfected with the luciferase reporter plasmids of *IL-6* and internal control plasmid (pGL4.74[hRluc/TK], Promega, China) for 24 h. Then the cells were lysed, and luciferase activity was measured using the Dual-Luciferase Reporter Assay System (Promega, China) according to the manufacturer's instructions.

IL-6 Chromatin immunoprecipitation (ChIP): ChIP assays were performed using SmapleChIP(R) Plus Kit (Magnetic Bead) (Cell Signal Technology, USA). Lysates were incubated with primary antibodies or negative control anti-IgG. The precipitated DNAs were analyzed and quantified by using RT-qPCR analysis. The primers for IL-6 promoter containing a p65 binding site were 5'-CGGTGAAG AATGGATGACCT-3' and 5'-AAACCAGACCCTTGCACAAC-3'.

Table 2
Forward and reverse primers for each gene.

Gene	Forward	Reverse
RELA	5′-GTGGGGACTACGACCTGAATG-3′	5′-GGGGCACGATTGTCAAAGATG-3′
IL-6	5′-ACTCACCTCTTCAGAACGAATTG-3′	5′-CCATCTTTGGAAGGTTCAGGTTG-3′
GAPDH	5′-GGAGCGAGATCCCTCCAAAAT-3′	5′-GGCTGTTGTCATACTTCTCATGG-3′

RELA: RELA proto-oncogene, NF-kB subunit; IL-6: interleukin 6; GAPDH: glyceraldehyde-3-phosphate dehydrogenase.

2.8. Synthesis of CSMA-PBA

CSMA-PBA was synthesized by esterification of CSMA with PBA. Briefly, 1 g of CSMA was dissolved in 0.1 M MES buffer to form a 1 % (w/v) solution. Then, 5 mL of 1 % PBA (w/v) dissolved in dimethyl sulfoxide (DMSO) was added. After thorough dissolution, 0.5 g of EDC and 0.7 g of NHS were added. The reaction was stirred at room temperature for 24 h. After the reaction, the solution was centrifuged at 7500 rpm for 0.5 h to remove unreacted PBA. Finally, the supernatant (MWCO 3500) was dialyzed against deionized water for 5 days and freeze-dried.

2.9. Preparation of OD-DA

As previously described, oxidized dextran (OD) was prepared using a periodate oxidation method. 1.50g of dextran was dissolved in 100 mL of distilled water to form a homogeneous solution. Then, 1.30g of sodium periodate was dissolved in 10 mL of water and added dropwise to the above solution. The mixture was stirred for 6 h in the dark at room temperature. Subsequently, 2 mL of ethylene glycol was added to terminate the reaction. The product was then dialyzed against water (MWCO 3500) for 3 days and freeze-dried.

Next, 1.00g of OD was dissolved in MES buffer solution at pH 5.5. Then, 0.95g of N-Hydroxysuccinimide (NHS) and 0.58g of 1-Ethyl-3-(3′-dimethylaminopropyl) carbodiimide (EDC) were added at room temperature and stirred for 30 min. Subsequently, 1.20g of dopamine was added under a constant temperature and stirred for 12 h under N2 atmosphere. The resulting product was dialyzed against distilled water (MWCO 3500) for 3 days and freeze-dried to obtain OD-DA.

2.10. Synthesis of CPDA hydrogel

Dissolve CSMA-PBA, OD-DA, and 2959 in water and polymerize under UV irradiation to form CPDA hydrogel.

2.11. Characterizations of hydrogels

The Fourier Transform infrared spectroscopy (FTIR): The FTIR experiments were carried out using a Nicolet iS10 FTIR Spectrometer (Thermo Fisher Scientific, Waltham, MA, USA) in a frequency range between 400 and 4000 cm-1. A total number of 32 scans with a resolution of 2 cm-1 were averaged for each spectrum.

The rheological characteristics of hydrogels: A rheometer (HR.1, TA Instrument, USA) was used to investigate the changes in modulus of the hydrogels under external forces. Initially, frequency sweep mode was selected with a strain of 1 %, and angular frequency varied from 1 rad/s to 100 rad/s to test the changes in storage modulus (G′) and loss modulus (G″). Subsequently, time sweep mode was chosen with a fixed angular frequency of 10 rad/s.

Swelling and degradation: The freeze-dried coatings were considered as the initial weight and labeled as WI. Subsequently, the samples were placed in PBS buffer. Every hour, the surface water of the hydrogels was removed using filter paper, weighed, and labeled as WS. The swelling ratio (SR) was calculated using the following formula:

Swelling Ratio = (WS - WI) / WI × 100%

In vitro drug release assay: Drug release was measured using ultraviolet absorbance. 0.1g of hydrogel was dissolved in 10 mL PBS. Every hour, 1 mL of supernatant was collected and replaced with 1 mL of PBS. UV spectrophotometry was used to quantify and analyze absorbance at $\lambda = 280$ nm. To characterize the pH-responsive properties of the hydrogels, they were placed in buffer solutions with pH 4.5 and 7.2 for 30 min. Subsequently, pH-responsive testing was performed using the method mentioned above.

Surface Morphology Analysis: Each group of hydrogels was frozen at -20 °C for 12 h and then subjected to freeze-drying to remove the water content. Scanning electron microscopy (SEM) was employed to observe the cross-sectional morphology of the hydrogels, studying the internal cross-linking network structure.

2.12. In vitro cytocompatibility and cytotoxicity of drug-loaded hydrogel

Cell Counting Kit-8 test: Cell Counting Kit-8 (CCK-8, APExBIO, USA) was applied to determine the cytotoxicity of SaB-loaded hydrogel (Sigma Aldrich, Germany). Synovial fibroblasts from the frozen shoulder patients were seeded onto 96-well plates at a density of 3000 cells per well and cultured with various concentrations of SaB. Subsequently, 10 µL of the CCK-8 reagent was added to each well at 24 h or 48 h, or 72 h after seeding and used to quantify the cell number after incubating for 1 h at 37 °C. All experiments were performed in triplicate. The absorbance at an OD of 450 nm was measured using a UV-spectrophotometer (Life Technologies, USA).

Live/dead assay: Live/Dead cell assay (Abbkine, China) was performed according to the manufacturers' protocol. Briefly, synovial fibroblasts were seeded in a 6-wellplate at a density of 5×10^4 cells per well and cultured overnight. Subsequently, fresh medium containing different concentrations of SaB-loaded hydrogels was used as a replacement. Cells were cultured for 24 h, then washed with PBS twice before staining. The staining solution was prepared by mixing 1 µL of LiveDye and 1 µL of NucleiDye in every 1 mL of Assay Buffer as staining solution. 100 µL of staining solution was added to cells and incubated at 37 °C for 15–30 min in the dark. Cells were visualized using fluorescence microscopy (Leica, Germany) immediately after washing cells with PBS twice. After fluorescence observation, the cells on the plate were harvested with trypsin and resuspended at 3×10^5/mL for flowcytometry.

ROS Scavenging Detection: The antioxidant activity of the hydrogels was assessed using a reactive oxygen species analysis kit (ROS analysis kit). First, L929 cells were cultured in DMEM medium containing 3 µg/mL H2O2 for 12 h. Then, the coating extracts were added to the culture medium and further incubated for 12 h. Subsequently, cells were stained with DCFH-DA solution (10 µM) for 20 min. Finally, images were captured using a fluorescence microscope to assess ROS clearance.

Antibacterial performance: Conducting antibacterial experiments using the plate count method. *Staphylococcus aureus* aureus and *Escherichia coli* are used as model bacteria and cultured in Luria-Bertani (LB) broth and brain-heart infusion (BHI) broth, respectively, at 37 °C. The bacterial solution is diluted to a concentration of 106 CFU/mL, and 1 mL of this solution is co-cultured with agar gel. Subsequently, the bacterial solution is serially diluted, and 100 µL of each dilution is spread onto solid culture medium and incubated at 12 °C for 48 and 72 h. The number of colony-forming units (CFUs) is recorded, and the absorbance at 600 nm is measured using a spectrophotometer.

2.13. In vitro antifibrotic effect of drug-loaded hydrogel

Western blotting: The expression of COL 1, COL 3, FN, α-SMA, IL-6, Nrf2, SLC7A11, GPX4, p65 and p-p65 were detected using western blotting and standardized to GAPDH.

Cell adhesion test: Cell adhesion ability was determined by cell-substrate adhesion assays as previously described [20]. Briefly, 100 µL of the adhesion substrate fibronectin (10 µg/mL; Sigma Aldrich, Germany) was added to flat bottom 96-well plates and incubated for 60 min at ambient temperature. Three wells were left blank to determine the background binding of crystal violet. Synovial fibroblasts from the frozen shoulder and healthy control group were pretreated according to different experimental conditions in 6-well plates and were subsequently harvested with trypsin and resuspended at 2.85×10^5/mL. Then, 50 µL cell suspension was added to 50 µL PBS prior to the addition of this cell suspension into the prepared wells. Synovial fibroblasts were allowed to adhere for 20 min at 37 °C in a 5 % CO2 incubator. Non-adherent cells were removed by tapping the plate gently and washing the wells twice with 100 µL PBS. Attached cells were fixed by using 100

μL of 5 % glutaraldehyde (Sigma Aldrich, Germany) and subsequently stained by adding 100 μL of 0.1 % crystal violet (Beyotime, China). Before dissolving the crystal violet, the cell adhesion morphology was captured by an inverted microscope (Nikon, Japan). The crystal violet dye was solubilized in 100 μL of 10 % acetic acid and the absorbance was measured at 570 nm using a UV-spectrophotometer (Life Technologies, USA). All experiments were performed in triplicate. The normalized absorbance was obtained by subtracting the background from the blank wells.

2.14. Animal model setup

The animal study was reviewed and approved by Institutional Animal Care and Use Committee, Sun Yat-Sen University (permit no: SYSU-IACUC-2023-001999). Thirty-six 12-week-old female Sprague-Dawley rats (200–300 g) were randomly divided into Group A: control group ($n = 9$), Group B: FS model group ($n = 9$), Group C: CPDA hydrogel injection group ($n = 9$) and Group D: SaB-CPDA hydrogel injection group ($n = 9$). In group B, C and D, rats were immobilized for 3 weeks to induce the FS. Immobilization procedures were conducted under intraperitoneal anesthesia using pentobarbital (30 mg/kg). The immobilization procedure was performed in the left shoulder of all rats. For the left shoulder, an approximately 2-cm skin incision was made on the medial border of the scapula, exposing the scapula and the humerus next to scapula. The scapula and humerus were tied using two 3-0 nylon sutures (Johnson & Johnson, Belgium), through the scapular bone and around the humerus shaft, to immobilize the glenohumeral joint [35]. After 3 weeks of immobilization, the sutures were removed in all rats in each group. In the group B, we applied 60 μL PBS to rats by intra-articular injection under CT guidance once a week, while an equal volume of CPDA hydrogel (60 μL) and SaB-CPDA hydrogel (60 μL, containing SaB at 50 mg/kg) was used in group C and D respectively. Each rat received ultraviolet light for 30 min to promote the formation of hydrogel in situ. Rats were used for gait analysis and then euthanized for measurement of the abduction angle and further histologic evaluation of the capsule after intervention of 3, 6, and 9 weeks.

2.15. In vivo fluorescence imaging

The SaB was labeled by Cy 5 dye before gelation. The labeled drug was mixed with unlabeled CPDA hydrogel (1:1) to form SaB-CPDA hydrogel at 10 wt%. Then 60 μL hydrogel was intra-articular injected into FS model rats. The whole-body fluorescence images were monitored immediately and at 1 d, 3 d and 7 d (IVIS Spectrum, PerkinElmer, USA).

2.16. Gait analysis

Gait analysis was performed by measuring the stride length of both sides between the front and rear paws on a grid paper [36]. The left-side paws of all rats were dabbed with a red-color inkpad, and the right-side paws were dabbed with a blue-color inkpad. Rats were made to walk on a grid paper by luring them with food. To make the rats walk straight, both sides of the grid paper were blocked with a wall. The distances between the front and rear paws on both sides were measured, and the longest distance of the measurement was defined as the stride length. This measurement was repeated 3 times in all rats, and the average was used for the analysis.

2.17. ROM evaluation

X-Ray examination: X-rays films of rats were acquired before euthanasia. Rats were positioned prone on a scanning table with tape just below the X-ray source under general anesthesia. The neutral and abduction positions' X-ray films were collected using a flatbed scanner. First, the rats' fore claws were naturally placed on both sides of the body, and the routine X-ray examination was performed to produce the neutral position X-ray film. Then fix the rats' fore claws with the No. 4 silk threads, while another end of which was tied to a 10 g weight. Place the rats prone on the X-ray inspection bed, fix both limbs in the abducted posture with the 10g weights suspended from both sides of the bed, and perform routine X-ray examination. Consider the axis of the humerus and the lateral edge of the scapula as the two sides of an angle with the humeral head's center as the vertex [37]. The calculation of angle was finished by using the system's own software and repeated by the same radiologist for 3 times, the average value of which was taken for further statistical analysis.

ROM in flesh: Each rat was euthanized under sufficient intraperitoneal anesthesia using pentobarbital (200 mg/kg) and, and the whole limbs from the scapula of whom were harvested en bloc. During the harvest, the origin and insertion of all muscles affecting the glenohumeral joint motion (deltoid, supraspinatus, infraspinatus, subscapularis, biceps, and triceps) were preserved, and extra care was taken not to damage the glenohumeral joint capsule. The scapula was fixed using two 27-G injection needles through the superior and inferior angles of the scapula on a Styrofoam block, thereby eliminating scapular motion. Further, the points on the distal end of the humerus when the shoulder was maximally adducted and maximally abducted were marked with 27-G injection needles. The angle between the scapular medial border and humerus shaft was measured using a protractor, and the glenohumeral ROM was calculated by subtracting the angle in a maximally adducted position from the angle in a maximally abducted position [36]. To avoid dehydration of soft tissue on the joint and to maintain reproducibility of each experiment, the whole procedure was performed within 15 min from the tissue harvest.

2.18. Histological evaluation

Part of the specimens used for ROM evaluation were immediately fixed in 10 % formalin for 16–24 h. The samples were then embedded in paraffin wax and sectioned into 3–5 μm for further hematoxylin and eosin (H&E) staining, Masson's trichrome staining and Sirus red stain (Solarbio, China) according to the manufacturer's protocol.

Immunohistochemistry (IHC): After deparaffinization and dehydration, the sections underwent antigen retrieval in citrate buffer, quenched in 3 % H_2O_2, and blocked with goat serum. The sections were further incubated with the specific antibody against IL-1β (Abcam, UK), IL-6 (Abcam, UK) and TNF-α (Abcam, UK) overnight at 4 °C. SP Rabbit & Mouse HRP Kit (DAB) (CW Biotech, China) were used to detect specific labeling according to the manufacturer's protocol.

2.19. Molecular biology analysis

The left of the specimens were used to collect the glenohumeral joint synovium/capsule tissue [38]. The anterior and posterior synovium/capsule tissue were carefully resected from the glenoid and humerus. The joint synovium/capsule tissues were then used for protein extraction and western blotting or ELISA. The expression of Fibronectin, COL 3, COL 1, Nrf2, SLC7A11 and GPX4 were detected. Also, the secretion of TGF-β1, PDGF, CTGF, IL-1β, IL-6 and TNF-α was evaluated.

2.20. Statistical analysis

Statistical analysis was performed with SPSS 23.0 software (Chicago, IL, USA). All data are presented as means ± standard deviations (SD). Student's t-test was performed to assess differences between two groups. P values < 0.05 were considered statistically significant.

3. Results and discussion

3.1. Differences in gene expression after SaB intervention

To clarify the underlying mechanism through which SaB attenuates

pathologic fibrosis, RNA-seq technology was employed to examine the synovial fibroblast transcriptome from 6 individuals with FS; 3 of these cells underwent SaB intervention.

In general, we identified 1623 differentially expressed genes (DEGs) with a fold change of ≥2 and an adjusted p-value of ≤0.001 between the SaB intervention and control groups. Among these, 837 were up-regulated, while 786 were down-regulated (Fig. 1B). The heat map and volcano plot of DEGs revealed the top 100 genes with the most significant differences in expression (Fig. 1A–C). Among the aforementioned DEGs, we focused on specific genes of interest, which we

highlighted using colored boxes. Fibrosis-related genes (highlighted with a blue box), such as COL1, COL4, COL5, COL6, and VIM, exhibited downregulation in the SaB intervention group. Conversely, MMP1, a gene known to promote collagen degradation, was upregulated, aligning with the findings from animal experiments. Furthermore, genes related to inflammation (indicated by a red box), including cytokine receptors, displayed alterations in expression. Intriguingly, we observed an upregulation of ferroptosis-related genes (highlighted with a green box), such as SLC40A1, SLC7A11, and SLC5A3, following SaB intervention. This suggests a potential link between fibrosis and ferroptosis. This may
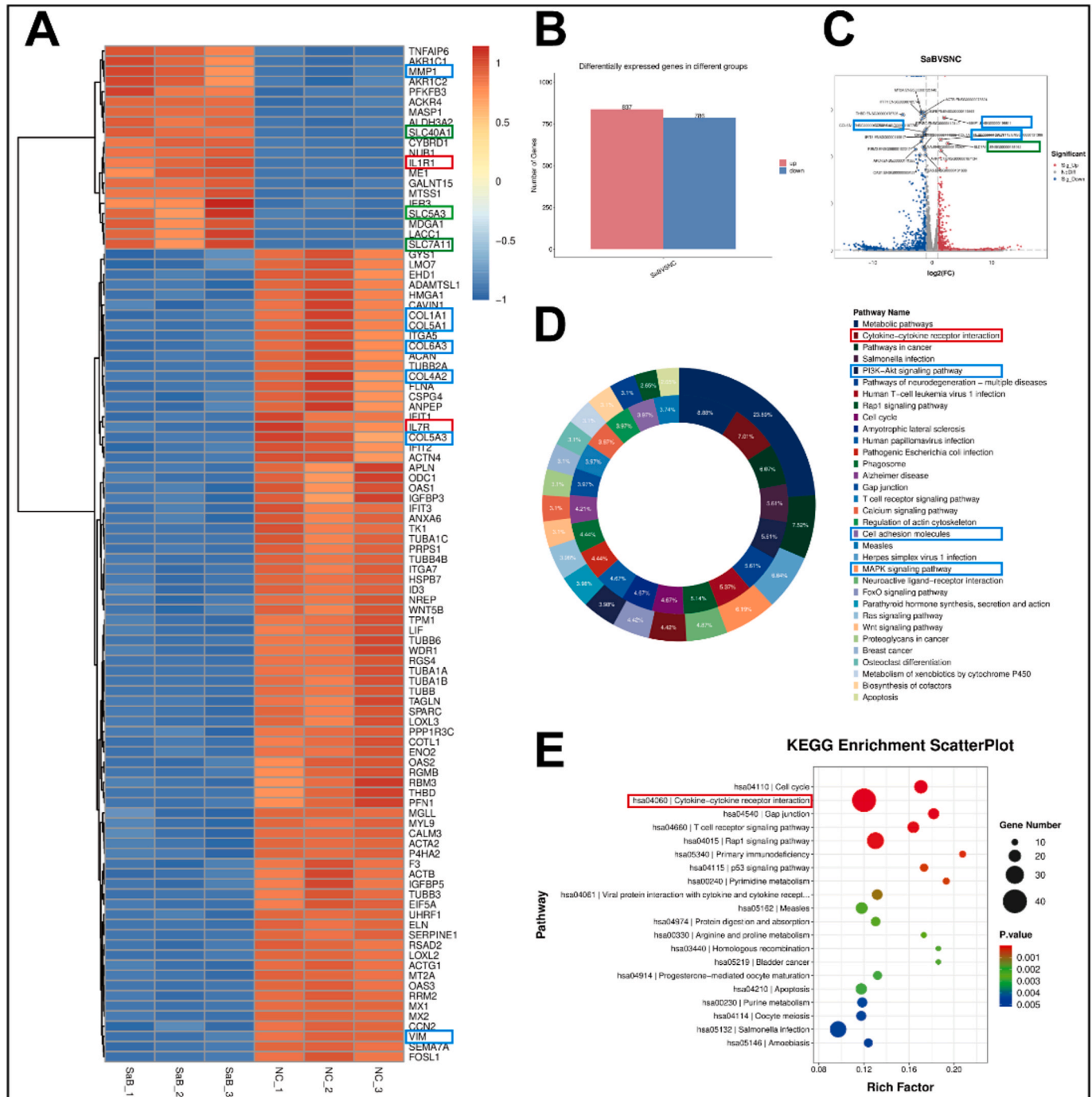

Fig. 1. Gene expression change of synovium fibroblasts after SaB intervention. A, B, C) A total of 1623 genes were differently expressed (Fold Change ≥2 and Adjusted p value ≤ 0.001) between SaB group and the control group, among which 837 were up-regulated and 786 were down-regulated. D, E) KEGG pathway analysis was performed to determine the pivotal signaling pathways within the differentially expressed genes. Rectangles were used to indicate the interested genes and pathways with fibrosis in blue, inflammation in red while ferroptosis in green.

indicate that there lies relationship between fibrosis and ferroptosis.

KEGG analysis was performed to determine the key signaling pathways related to the DEGs; all significant signaling pathways are shown in Fig. 1D and E. Among these pathways, the Cytokine-cytokine receptor interaction pathway (highlighted with a red box) exhibited the most significant changes. This strongly indicates that inflammation may be a pivotal factor in the relationship between SaB intervention and synovial fibroblast-induced fibrosis. It's noteworthy that in our previous research, we established that IL-6 promotes synovial fibroblast-induced fibrosis by activating the PI3K-Akt signaling pathway [22]. In contrast, SaB has been shown to attenuate fibrosis by inhibiting the CD36-mediated activation of the PI3K-Akt signaling pathway [28]. Notably, the PI3K-Akt signaling pathway was also identified in the KEGG enrichment plot, alongside Cell adhesion molecules and the MAPK signaling pathway (highlighted with a blue box), all of which have been previously reported to be associated with fibrosis. Consequently, we speculate that SaB exhibits anti-fibrotic, anti-inflammatory, and anti-oxidative effects on synovial fibroblasts, with cytokines potentially playing a pivotal role in mediating these effects.

3.2. SaB attenuates ferroptosis in synovial fibroblasts

Given the RNA-seq analysis results suggesting significant alterations in the expression of genes related to ferroptosis, further experiments were conducted to assess the extent of ferroptosis in SFs. Erastin was applied for 48 h to induce ferroptosis, while SaB was used to inhibit lipid peroxidation in SFs. Fig. 2A indicates no significant difference in Nrf2 expression between cells treated with SaB or erastin according to western blotting results ($p > 0.05$). Besides, elevated expression of SLC7A11 was detected in SaB intervention group compared to erastin intervention group ($p < 0.01$). Furthermore, GPX4 expression in the SaB intervention group was significantly higher than in the other three groups ($p < 0.05$). Moreover, the MDA levels exhibited a sharp decrease following erastin intervention, and this trend was subsequently reversed by SaB, as indicated by the MDA assay (Fig. 2B). The BODIPY 581/591C11 kit was also utilized to detect lipid ROS in SFs. Erastin was still used as an inducer of ferroptosis, while fer-1 served as its inhibitor. Both SaB and fer-1 demonstrated remarkable anti-lipid ROS capabilities regardless of the presence of erastin; however, no synergistic anti-oxidative effects were observed between them (Fig. 2C and D). In general, it has been demonstrated that SaB can attenuate ferroptosis in synovial fibroblasts. Nevertheless, further research is required to elucidate the relationship between ferroptosis and fibrosis.

3.3. SaB induces macrophage polarization towards M2 type

The sequencing results have sparked our particular interest in the role of inflammatory cytokines and their associated factors in FS development. According to the literature, synovial fibroblasts and synovial macrophages are the main cell types found in the synovium of the shoulder joint. Macrophages may serve as the source of the inflammatory cytokine cascade. Also, Macrophages play a role in FS development and progression through different polarization types, including M1 and M2 [39]. Therefore, experiments were conducted to investigate the impact of SaB on macrophage polarization.

IFN-γ with LPS was employed to induce polarization of RAW 264.7 cells towards the M1 type, while IL-4 was used to induce polarization towards M2, serving as positive controls [40]. After 48 h of SaB administration, the macrophages underwent a morphological change from oval to polygonal shape with short antennae (Fig. 2E). The flow cytometry results indicated a significant increase in CD86(−) CD206 (+) cells in the SaB group compared to the negative control, suggesting a shift towards M2 polarization as the dominant direction (Fig. 2F).

However, there is still uncertainty regarding the effects of macrophage polarization in different directions on the pathologic fibrosis process. We seeded polarized RAW 264.7 cells into the lower transwell chamber and SFs into the upper chamber, allowing them to co-culture for 24 h. The M2 and SaB groups exhibited fewer migrated cells in the transwell assay compared to the M1 and control groups (Fig. 2G and H). Subsequently, SFs were cultured in the macrophage medium and lysed for western blotting analysis. Consistent with the transwell assay results, significantly lower levels of fibrosis-related proteins, including FN, COL1, COL3, and α-SMA, were observed in the M2 and SaB groups (Fig. 2I). SaB has the potential to mitigate pathologic fibrosis by inducing macrophage polarization towards the M2 type.

3.4. SaB prevent fibrosis by inhibiting NFκB/IL-6 inflammatory pathway

Sequencing results indicated that the interaction between cytokines and their receptors was the most significant pathway following SaB intervention, as evidenced by the low p-value and high enrichment factors. The NFκB pathway played a pivotal role in this context [41]. Our prior research has established that IL-6 plays a vital role in frozen shoulder by mediating the progression of pathological fibrosis through the PI3K/Akt pathway [22]. Additionally, SaB has been shown to reduce the expression of several inflammatory cytokines in fibroblasts in vitro, particularly IL-6 [28]. Consequently, it is essential to further explore the associations between SaB and NFκB/IL-6 in fibroblasts, the interactions involving NFκB and IL-6, and the implications of NFκB/IL-6 in the development of pathological fibrosis in FS.

In the initial phase, we investigated the impact of SaB on the expression of NFκB and IL-6. The results of Western blotting showed that the indexes related to fibrosis decreased gradually with the increase of SaB concentration, accompanied by p-p65 and IL-6 (Fig. 3A). These findings were corroborated by ELISA experiments, where IL-6 secretion in the culture medium exhibited a consistent decline with rising SaB concentrations (Fig. 3B). To elucidate the connection between NFκB/IL-6 and FS, we conducted IF staining on shoulder synovium sections from both FS patients and healthy controls. IF results indicated a significantly elevated expression of pp65 and IL-6 in the synovium of the FS group compared to the control group ($p < 0.01$, $p < 0.05$, respectively; Fig. 3C). Subsequently, cellular-level IF detection was performed after 24 h of incubation with a polarized macrophage culture medium. P65 IF staining on synovial fibroblasts revealed distinct nuclear penetration, as observed through a confocal microscope. The degree of p65 entering the nucleus was assessed, considering literature support affirming that p65 exerts its biological effects in the nucleus. Broadly, the M1 group exhibited the highest nuclear penetration, the M2 group the least, and the SaB group slightly below the M2 group (Fig. 3D). In essence, the NFκB/IL-6 pathway and fibrosis levels were attenuated following SaB intervention.

In our pursuit to delve deeper into the intricate relationship between NFκB and IL-6 within fibroblasts, we meticulously modulated the expression of p65. Initially, the small interfering RNAs targeting RELA (siRELA) were transfected into the cells. We meticulously assessed the knockdown efficiency through qRT-PCR and western blotting analysis. Notably, siRELA2 exhibited the most robust knockdown efficiency, resulting in a substantial downregulation of IL-6 expression (Fig. 3E and F). To comprehensively affirm the intricate interplay between these entities, we conducted double luciferase experiments focusing on IL-6. The outcomes were compelling: the siRELA group exhibited a pronounced reduction in IL-6 transcription levels, while overexpression of p65 via the oeRELA plasmid led to a marked upregulation in IL-6 transcription. Furthermore, our ChIP assay targeting IL-6 provided crucial insights. It clearly demonstrated NFκB's specific binding to the IL-6 promoter within the nucleus (Fig. 3G and H). Notably, SaB significantly attenuated this binding, further emphasizing NFκB's regulatory role upstream of IL-6.

The relationship between NFκB/IL-6 and fibrosis merits our careful attention and thorough examination. To address this issue, we conducted additional experiments employing western blotting and cell adhesion assays. As illustrated in Fig. 4A and B, both IL-6 intervention
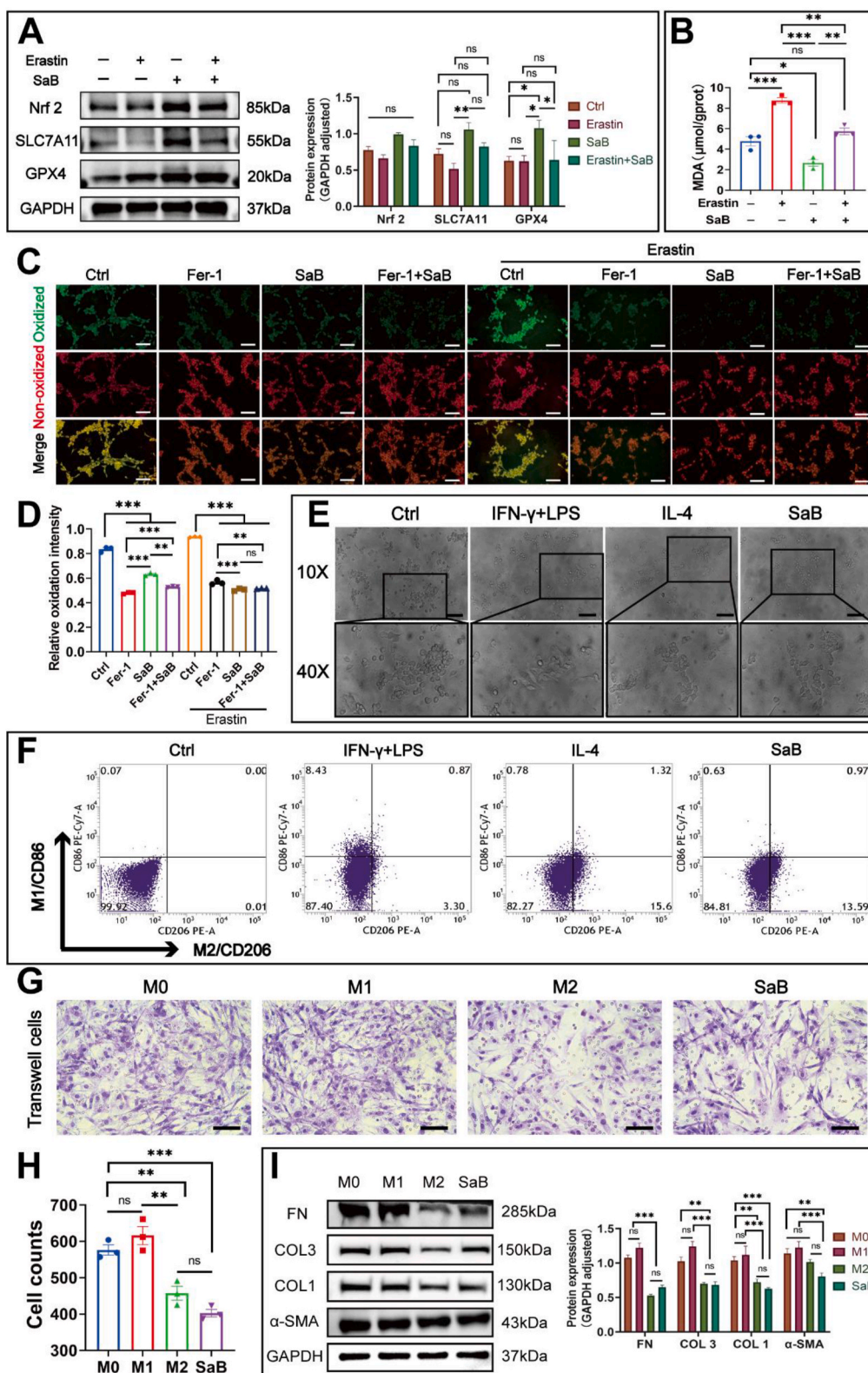
Fig. 2. SaB attenuates ferroptosis and induces macrophage polarization towards M2 type. A) Western blotting results showed that SaB attenuates erastin-induced ferroptosis in synovial fibroblast with increased expression of Nrf 2, SLC7A11 and GPX4. B) MDA assay suggested decreased level of lipid peroxidation after SaB administration. C, D) BODIPY 581/591C11 kit was used to detected lipid ROS in synovial fibroblasts. SaB showed considerable anti-oxidation ability as ferroptosis inhibitor Fer-1 did. Scale bar: 50 μm. RAW 264.7 cells polarized towards M2 type after cultured with SaB for 24 h according to morphology under microscope (E) and flowcytometry (F). Scale bar: 50 μm. G, H) Synovial fibroblasts were seeded into the upper chamber and co-cultured with RAW 264.7 cells in the lower chamber for 24 h. The amount of transwell cell were calculated to show fibrosis-related ability. Scale bar: 100 μm. I) Western blotting results suggested that less fibrosis related protein including FN, COL 1, COL 3 and α-SMA was detected in synovial fibroblasts cultured with medium obtained from macrophages culture system in M2 and SaB group. *P < 0.05; **P < 0.01; ***P < 0.001.
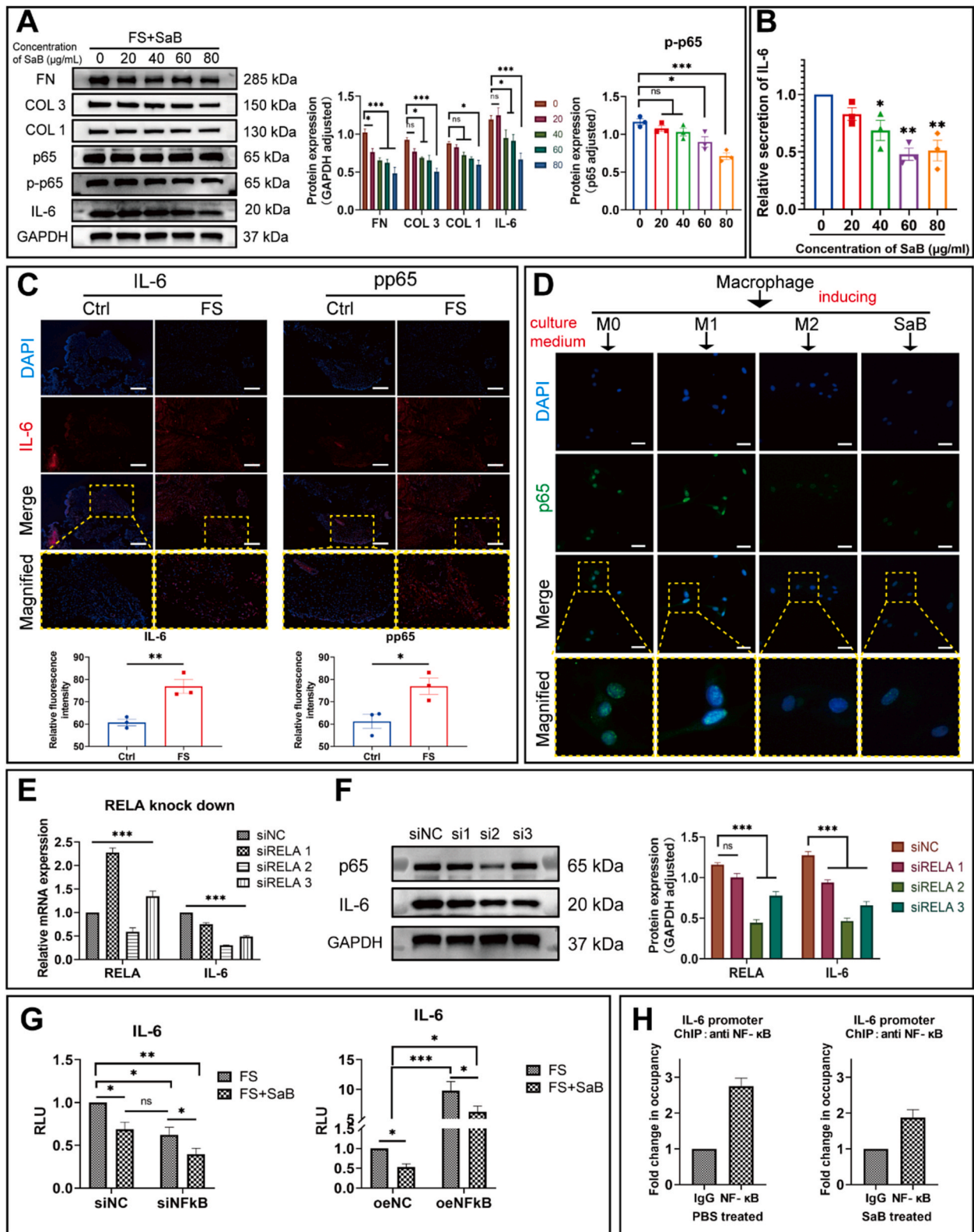
Fig. 3. SaB inhibiting NFκB/IL-6 signaling pathway. A) Western blotting results showed that as the concentration of SaB increased, synovial fibroblast expressed less fibrosis-related proteins including FN, COL 1 and COL 3, as well as IL-6 and p-p65. B) ELISA assay suggested decreased secretion of IL-6 in synovial fibroblasts after SaB intervention. C) IF image showed that the expression of pp65 and IL-6 in synovium of FS group was significantly higher than that of control group. Scale bar: 200 μm. D) IF image captured using co-focus microscope reminded that less p65 was detected in nucleus of synovial fibroblasts co-cultured with macrophages M2 and SaB group. Scale bar: 50 μm. E, F) *RELA* knockout efficiency verification using qRT-PCR and western blotting. Decreased expression of IL-6 was detected after RNAi. G) Double luciferase experiment of IL-6 showed that the transcription level of IL-6 in *siRELA* group was significantly down-regulated, but up-regulated after over-expression of *RELA*. H) ChIP assay for IL-6 suggested that NFκB could specifically bind to the promoter of IL-6 in the nucleus, while the process of which could be inhibited by SaB. *P < 0.05; **P < 0.01; ***P < 0.001.
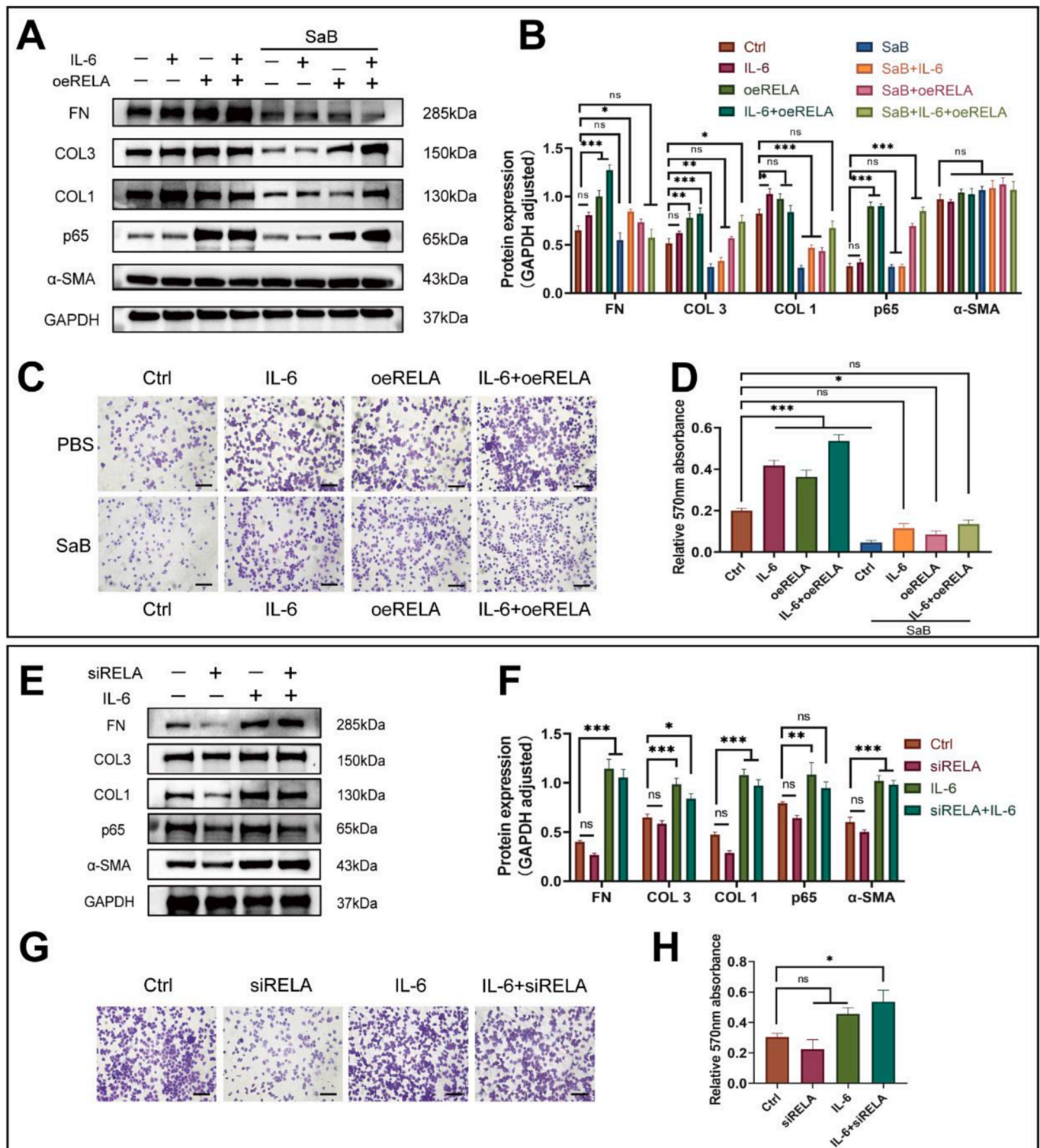
Fig. 4. SaB prevent fibrosis by inhibiting NFκB/IL-6 inflammatory pathway. A, B, C, D) Western blotting and cell adhesion assay results showed that both the administration of IL-6 and overexpression of RELA could counteract the anti-fibrosis effect of SaB in synovial fibroblast. E, F, G, H) Western blotting and cell adhesion assay results showed that the administration of IL-6 could counteract the anti-fibrosis effect of knocking down RELA in synovial fibroblast. Scale bar: 50 μm *P < 0.05; **P < 0.01; ***P < 0.001.

and the overexpression of NFκB via oeRELA counteracted SaB's anti-fibrotic suppression. They effectively elevated the expression levels of fibrosis-related proteins, demonstrating a certain synergistic effect. The statistical analysis of the final count of adherent cells in the cell adhesion assay corroborated these findings (Fig. 4C and D). Subsequent experiments revealed that siRELA reduced the expression of fibrosis-related

proteins and impaired the adhesion capacity of fibroblasts by diminishing NFκB expression. Notably, this effect could be reversed by IL-6 (Fig. 4E–H). In summary, the NFκB/IL-6 pathway plays a pivotal role in fibrosis. When combined with previous research, it suggests that SaB can attenuate the signaling of the PI3K/Akt pathway by inhibiting the NFκB/IL-6 pathway, thereby exerting an anti-fibrotic effect in FS.

3.5. Design, synthesis and characterizations of drug-loaded hydrogel

The synthetic route of CPDA hydrogel is shown in Figure Scheme. The simple drug release system cannot cope with the development of inflammation and changes in the body's microenvironment. An ideal drug delivery system should possess "intelligence," enabling adaptive adjustments and feedback in response to microenvironmental changes. In the frozen shoulder lesion area, the deficiency of intracellular or microenvironmental antioxidants such as glutathione (GSH) and superoxide dismutase (SOD) is insufficient to eliminate the excessive
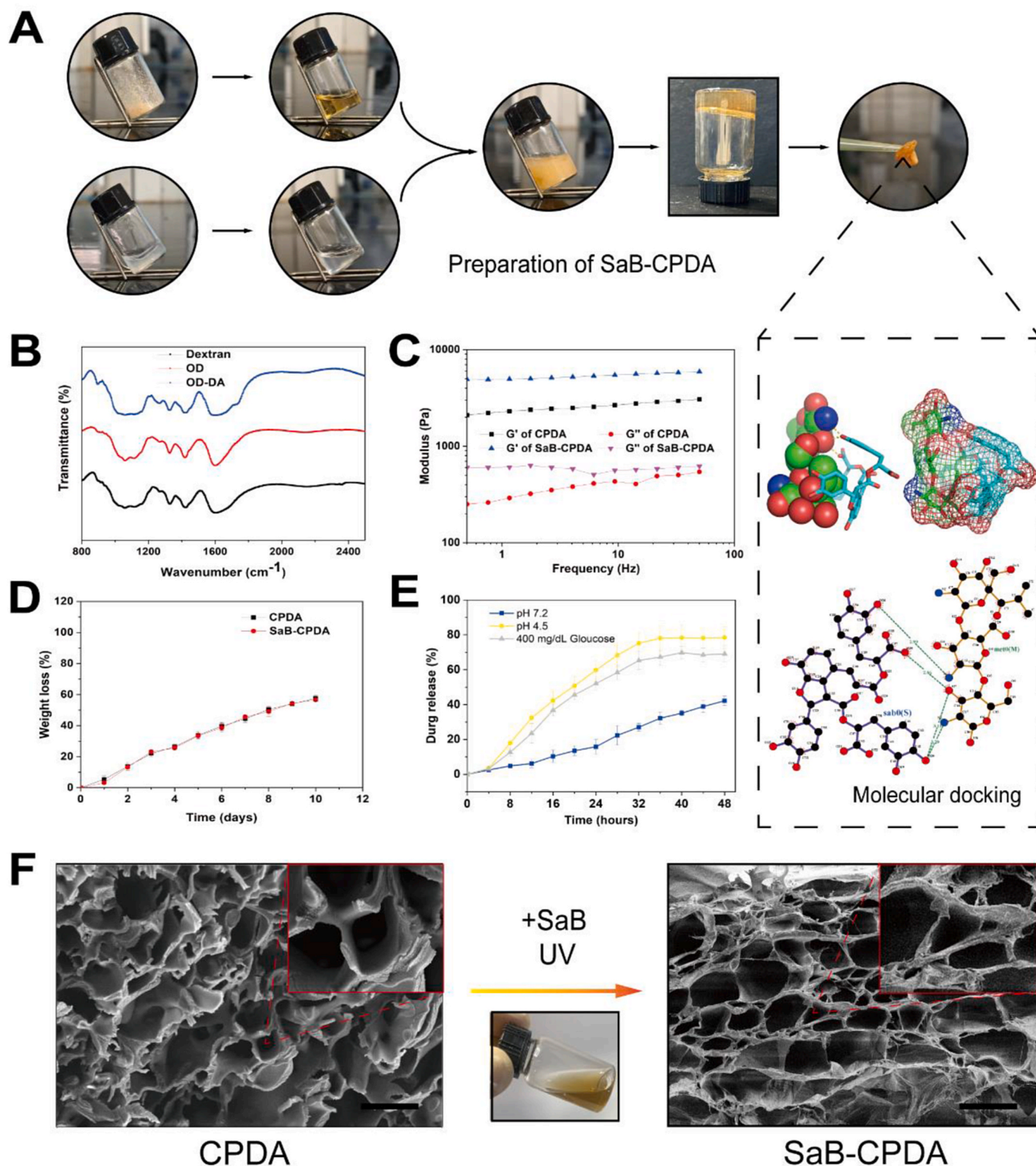

Fig. 5. Preparation and characterization of CPDA and SaB-CPDA. A) The preparation and autodocking simulation of SaB-CPDA. B) FTIR spectrum of Dextran, OD, and OD-DA. C) Rheological time sweep of CPDA and SaB-CPDA (SaB: 2 wt%). D) In vitro degradation curve of CPDA and SaB-CPDA, the loading of SaB did not show a statistically significant difference in degradation of hydrogel (SaB: 2 wt%). E) SaB drug releasing behavior with excellent pH responsiveness in vitro (SaB: 2 wt%). F) TEM morphology of CPDA and SaB-CPDA (SaB: 2 wt%). Scale bar: 5 μm *$P < 0.05$, **$P < 0.01$, ***$P < 0.001$.

production of ROS. This imbalance triggers metabolic disruptions and biomolecular damage, ultimately leading to cell apoptosis.

It has been demonstrated that there existed a significant increase in ROS levels in the joints of FS patients. Oxidative stress resulting from excessive ROS production leads to chondrocyte membrane damage and synthesis of the protein-polysaccharide matrix. ROS-induced activation of the NF-κB pathway halts chondrocyte growth and promotes the secretion of MMP, exacerbating cartilage inflammation. As aging progresses, chondrocytes become increasingly sensitive to ROS damage, inducing more cell senescence and apoptosis [42]. Furthermore, ROS clearance can effectively alleviate pathologic fibrosis in joint. Zhang et al. recently synthesized ROS-responsive materials with excellent mechanical properties [43]. In comparison to the control, this material underwent a dramatic morphological transformation after incubation with hydrogen peroxide, with all thioester bonds being disrupted, leading to nanoparticle dispersion and structural relaxation. In in vivo experiments, this material not only demonstrated good joint targeting but also facilitated the transition of synovial macrophages to the M2 type, downregulating the expression of MMP-2 and various inflammatory factors in joint cartilage. These findings suggest an intimate connection between abnormally elevated ROS and the pathological progression of FS, indicating that utilizing high levels of ROS in the FS tissue microenvironment is a promising trigger for reactive drug release. Therefore, we introduced ROS-sensitive boronate ester bonds into the hydrogel to respond to changes in the microenvironment.

To analyze the crosslinking status of CPDA and SaB, we utilized software to simulate the loading of water-soluble SaB through the CSMA main chain. The results indicate a substantial presence of hydrogen bonds between the two chains, signifying the successful incorporation of SaB within the hydrogel and establishing the groundwork for subsequent controlled release (Fig. 5A).

The OD-DA polymer was synthesized via an amide bond reaction in the presence of EDC/NHS. Fig. 5B illustrates the infrared test results, confirming the successful synthesis of the polymer. CPDA hydrogel polymerization was completed in 30 s under UV. Furthermore, the morphology of the freeze-dried hydrogel was observed using SEM, revealing a typical interconnected and porous microstructure (Fig. 5F).

To analyze the rheological properties of the hydrogel and evaluate its mechanical behavior, frequency sweep curves show that the hydrogel has stable G′ values greater than G″ in the range of 0.1–50Hz (Fig. 5C). Moreover, upon loading SaB, both G′ and G″ of the hydrogel increased, indicating enhanced crosslinking. Additionally, we tested the degradation behavior of the hydrogel. Fig. 5D illustrates the gradual degradation of the hydrogel over time, resulting in a 50 % reduction in mass after 10 days. Moreover, the loading of SaB did not exhibit a statistically significant difference in the degradation curve of the hydrogel.

In conventional drug delivery methods, drugs are directly mixed with sterile gauze or hydrogel, a simple and convenient approach that, however, has numerous limitations. More specifically, functionally loaded drugs are quickly released or absorbed by the gauze, rendering them biologically ineffective. This, in turn, reduces the drug's duration of action, preventing it from achieving the goal of long-term sustained efficacy in the diseased area. In our system, water-soluble SaB is encapsulated within the CPDA hydrogel, providing a controlled, slow release over time. As depicted in Fig. 5E, after 48 h in a PBS solution with a pH of 7.2, drug release reaches 38 %, whereas in a pH 4.5 solution, drug release reaches 79 %. This suggests that the hydrogel exhibits outstanding pH responsiveness, facilitating improved drug release in the inflamed area.

3.6. In vitro safety and anti-oxidation ability evaluation

Intra-articular injection hydrogels must exhibit excellent biocompatibility. To assess the in vitro safety of the SaB hydrogel, SFs were isolated from synovial tissues obtained from FS patients and cultured following our prior methodology. Subsequent experiments were conducted using these synovial fibroblasts. he cytotoxicity of the SaB hydrogel was assessed using a CCK-8 assay. Typically, higher concentrations of SaB were correlated with a reduced count of viable SFs. A significant difference was observed at a concentration of 80 μg/mL at both 48 h and 72 h (Fig. 6B). The cell viabilities of all experimental groups exposed to various SaB concentrations (0, 20, 40, 60, and 80 μg/mL) did not differ significantly from the control group, as indicated by the Live/Dead cell assay results. All groups exhibited comparable Live/Dead staining patterns in fluorescence images (Fig. 6C), which corroborates the findings from flow cytometry (Fig. 6D). Consequently, SaB concentrations below 80 μg/mL appeared to exert no significant impact on the growth and proliferation of SFs within 72 h and were therefore selected for further investigation. Additionally, SaB-CPDA exhibited superior anti-oxidation and anti-bacterial ability when compared to the control group and the CPDA hydrogel group (Fig. 6E and F). In general, SaB-CPDA hydrogel showed excellent biocompatibility and anti-oxidation effect in vitro.

3.7. In vitro regulation of fibrosis-related ability in synovial fibroblasts

The ability of synovial fibroblasts to produce and secrete ECM is crucial in pathological fibrosis, and this also influences their cell adhesion function. To demonstrate the anti-fibrotic effect of SaB-CPDA, we used Western blotting and cell adhesion tests to assess the fibrosis-related functions of synovial fibroblasts in various groups. In general, higher concentrations of SaB were associated with reduced adhesion function and lower expression of Fibronectin, COL1, and COL3 in synovial fibroblasts. The lowest level of healing was observed at a concentration of 80 μg/mL (Fig. 6G–K). Interestingly, the count of adhered cells seemed slightly lower in the 40 μg/mL group compared to the 60 μg/mL group, possibly because the cell culture time was insufficient for complete SaB release from the hydrogel. Furthermore, IL-6 has been reported to be associated with FS development and appeared to decrease significantly as the SaB concentration increased, consistent with our previous findings. The aforementioned results suggest that the SaB hydrogel has the potential to mitigate synovial fibroblasts-induced fibrosis in vitro.

3.8. In vivo regulation of hydrogel degradation and drug release

Experiment animals weighing 200–300 g were randomly divided into four groups. Rats in group An underwent sham operations, while rats in the other three groups underwent FS model establishment surgeries involving scapula-humerus ligation (Fig. 7A). All the model rats received weekly intra-articular injections in the shoulder using either PBS (group B), CPDA hydrogel (group C), or SaB-CPDA hydrogel (group D), guided by CT navigation and underwent ultraviolet light for 30 min to promote the formation of hydrogel in situ. The development of pathological fibrosis and chronic inflammation is an ongoing process. Currently, the optimal residence time of intra-articular injection hydrogel remains uncertain and requires further investigation. Therefore, we utilized four healthy rats for in vivo fluorescence imaging to assess hydrogel degradation and drug release in the shoulder. In vivo imaging was observed from day 1 to day 7 with Cy5-labeled SaB (utilized in both SaB solution and SaB hydrogel injections, Fig. 7B). The results demonstrated that the SaB-CPDA hydrogel exhibited long-lasting presence in the shoulder cavity, whereas SaB alone exhibited a weak signal after 7 days. No fluorescence signal was detected in the sham control and PBS injection groups. The prolonged retention of the SaB hydrogel suggests that using CPDA hydrogel as a carrier for SaB reduced the initial burst release and extended the release duration.

3.9. Effects on ROM of model rats

Limited ROM and worsening pain in shoulder are the key symptoms of FS. Following a 9-week regimen of intra-articular injections, ROM in
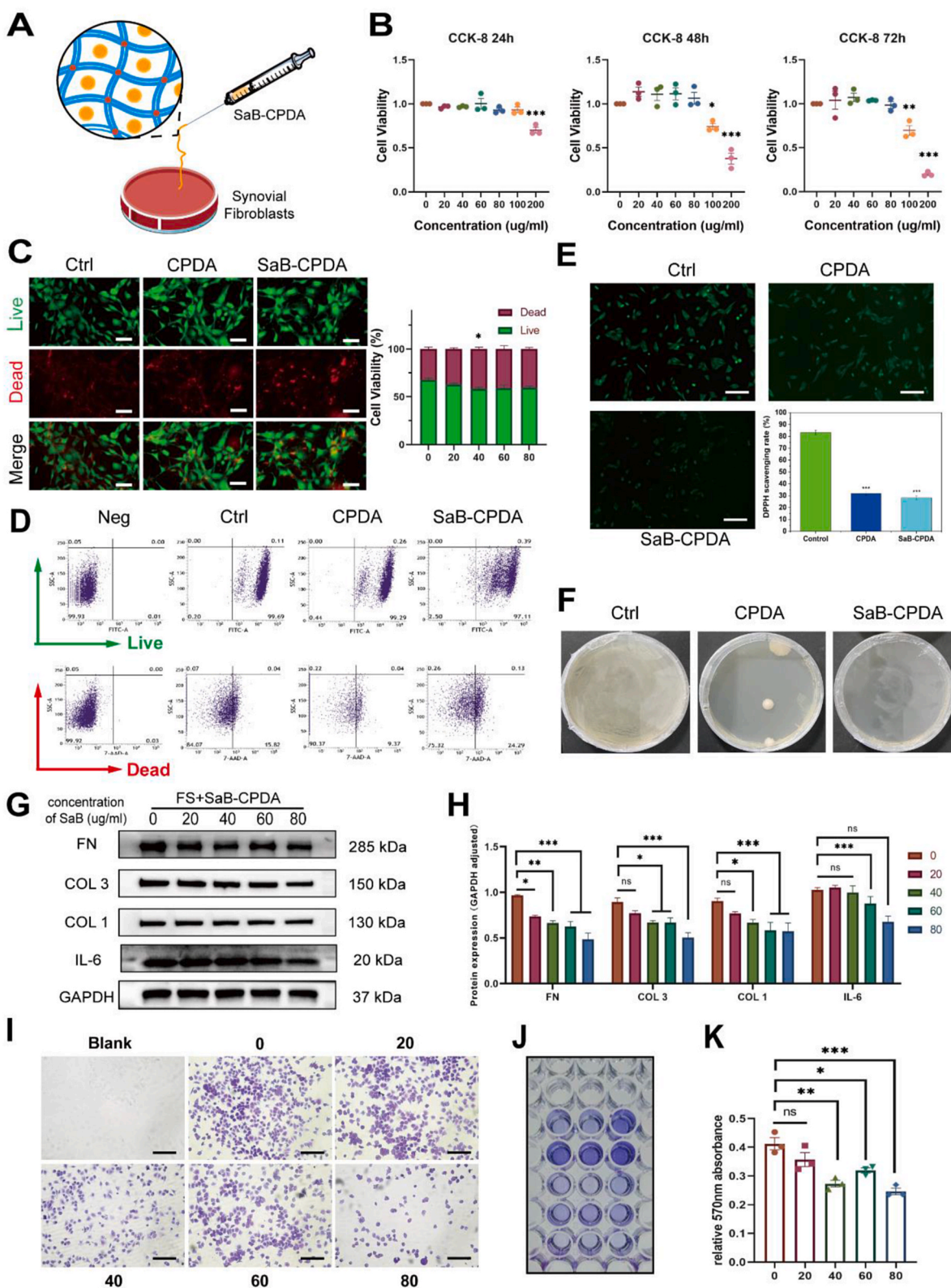
Fig. 6. In vitro Safety, anti-oxidation, anti-bacterial and anti-fibrotic ability evaluation. A) Injection of SaB-CPDA into culture medium for synovial fibroblasts. B) CCK-8 test for synovial fibroblasts cultured with SaB-CPDA consisted of a range of SaB concentrations (0, 20, 40, 60, 80, 100 and 200 μg/mL) (n = 3). C) Live/Dead staining of synovial fibroblasts after 48 h of co-culture with the hydrogels (n = 3). Scale bar: 50 μm. D) Flowcytometry of Live/Dead staining (n = 3). E) ROS Scavenging Detection of synovial fibroblasts cultured with hydrogels for 12 h using DCFH-DA solution (n = 3) Scale bar: 50 μm. F) Antibacterial analysis of hydrogels. Digital photographs of S. aureus colonies after incubating with hydrogels for 48 h. G, H) Western blotting results showed that as the concentration of SaB increased in hydrogel, synovial fibroblast expressed less fibrosis-related proteins including FN, COL 1 and COL 3, as well as IL-6. I, J, K) Cell adhesion test suggested that SaB-CPDA inhibiting the fibrosis-related functions of synovial fibroblasts (n = 3). Scale bar: 50 μm *P < 0.05, **P < 0.01, ***P < 0.001.
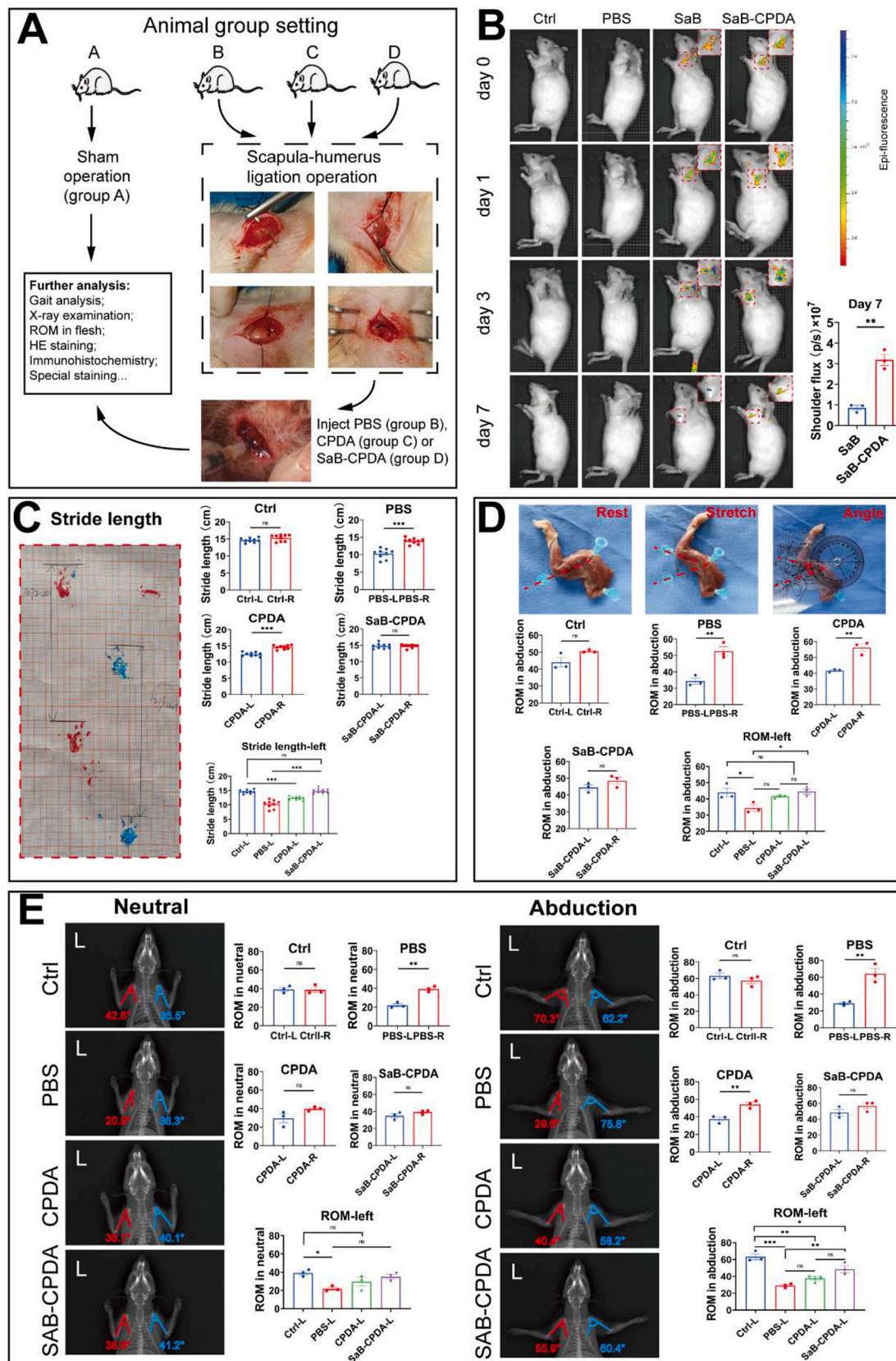
Fig. 7. SaB-CPDA blocks the progression of pathologic fibrosis of frozen shoulder in vivo. A) Animals were divided into four groups for further experiments. B) In vivo imaging of intra-articular injection of Cy5-SaB-CPDA on model rats (50 μL). C) Gait analysis by measuring the stride length on a grid paper. Stride length is defined as the longest distance between the front and rear paws. D) Evaluation of the shoulder ROM in flesh. E) The neutral and abduction positions' X-ray films were collected using a flatbed scanner. ROM was calculated on radiograph. *P < 0.05; **P < 0.01; ***P < 0.001.

SD rats was assessed.

Gait analysis was performed after removing the suture for fixation in left shoulder. Groups B and C had significantly decreased stride length on the left compared to the right side (10.26 ± 0.47 cm vs. 13.91 ± 0.28 cm, 12.42 ± 0.20 cm vs. 14.42 ± 0.20 cm, respectively; $p < 0.001$), whereas group A and D showed no difference in stride length between both sides (all $p > 0.05$). In between-group analyses of the left immobilized shoulders, group B showed a significantly smaller stride length on the left than the other 3 groups, while group C smaller than group A and D (14.62 ± 0.22 cm in group A, 10.26 ± 0.47 cm in group B, 12.42 ± 0.20 cm in group C and 14.76 ± 0.27 cm in group D, $p < 0.001$, respectively). Interestingly, no significant difference between group A and D was found ($p > 0.05$) (Fig. 7C). FS rats treated with SaB-CPDA hydrogel injection showed a significantly larger stride length compared to the sham control and PBS injection only groups.

To evaluate the ROM of shoulder, radiographical image was applied. X-ray films of the rats in neutral or abduction position were obtained under general anesthesia. In neutral position, significant differences were found between both shoulders in group B ($22.00° \pm 1.72°$ in the left vs. $39.38° \pm 1.68°$ in the right, $p < 0.01$). Besides, group B showed a significantly smaller ROM on the left than the group A ($22.00° \pm 1.72°$ vs. $39.25° \pm 2.17°$, $p < 0.05$). Additionally, significantly different ROM in abduction was found between the immobilized and control shoulders in groups B and C ($29.07° \pm 1.45°$ vs. $64.15° \pm 6.26°$, $37.56° \pm 2.47°$ vs. $54.34° \pm 2.51°$, respectively; $p < 0.01$). There was no difference in abduction between both shoulders in group A and D. In between-group analyses of the left immobilized shoulders, group B had a significantly lower ROM than groups A and D, but similar with that in group C ($63.31° \pm 3.48°$ in group A, $29.07° \pm 1.45°$ in group B, $37.56° \pm 2.47°$ in group C and $48.47° \pm 4.00°$ in group D, respectively); there was also a significant difference between groups A and D ($p < 0.05$) (Fig. 7E).

The rats were then euthanized for further research. The abduction angle on fresh cadaver specimens were measured; a significant difference in shoulder ROM was observed between the left immobilized and right control shoulders in groups B and C ($34.33° \pm 1.86°$ vs. $52.67° \pm 2.73°$, $41.67° \pm 0.60°$ vs. $56.17° \pm 2.35°$, respectively; $p < 0.01$). However, no similar difference was detected in group A and D (all $p > 0.05$). In the between-group analyses, group B showed significantly smaller ROM than groups A and D, but similar with that in group C ($44.00° \pm 4.77°$ in group A, $34.33° \pm 1.86°$ in group B, $41.67° \pm 0.60°$ in group C and $44.50° \pm 1.61°$ in group D respectively). However, there was no difference in the left shoulder ROM between groups A and D ($p > 0.05$) (Fig. 7D). These findings indicate that FS rats treated with SaB-CPDA hydrogel had a significantly greater ROM compared to control animals treated with PBS solution or CPDA hydrogel.

3.10. Assessment of pathologic fibrosis, ferroptosis and inflammation in vivo

Since the in vitro safety of SaB-CPDA hydrogels has already been demonstrated using synovial fibroblasts, H&E staining was performed on slices of internal organs from experimental rats to assess the in vivo toxicity of SaB-CPDA hydrogels. In general, no significant pathological changes were observed in heart, liver, spleen, lung, or kidney slices from all groups of animals (Fig. 8A).

Therefore, shoulder joint slices were employed to assess infiltration of inflammatory cells and pathological fibrosis using H&E staining, Masson's trichrome staining, and Sirus red staining. In H&E staining, we quantified macrophage infiltration in the region of interest near the axillary capsule of the shoulder joint by counting macrophages at high magnification. In Masson's trichrome staining images, the region of interest was centered around the axillary bursa of the shoulder joint to assess the overall appearance of pathological fibrosis. Yellow lines were used to delineate the region of interest in the axillary bursa, and measurements of the thickened region (indicated by red arrows) and the overall area were calculated for further analysis of thickness and fibrosis

in the shoulder capsule, following established research methods. Additionally, for the Sirus red staining images, a polarized light microscope was utilized to capture and analyze the localized deposition of COL 1 and COL 3.

In Batch 1, all rats received intervention for 3 weeks after removing the fixation in left shoulder. In the in three groups of rats undergoing FS inducing surgery, significantly increased number of macrophages were found in axillary capsule ($p < 0.05$). No significant difference of thickness or fibrosis area was found between 4 groups. Also, all groups showed similar distribution of COL 1 and COL 3 (Fig. 8B and C). In Batch 2, all rats received intervention for 6 weeks after removing the fixation in left shoulder. Groups B and C were associated with significantly increased infiltration of macrophages and thickened of axillary capsule on the left compared to the control group ($p < 0.05$). And increased fibrosis area was detected in all 3 model groups compared to group A ($p < 0.01$). However, only group C showed significantly more deposition of COL 1 between than group A in the Sirus red staining image (Fig. 8D and E). In Batch 3, all rats received intervention for 9 weeks after removing the fixation in left shoulder. No significant difference of macrophage counts was found between 4 groups. Groups B and C had significantly increased thickness of axillary capsule on the left compared to the control group ($p < 0.001$, $p < 0.05$, respectively). Increased fibrosis area was found in groups B, C and D compared to group A ($p < 0.001$). In addition, group B and C showed increased COL 1 deposition than group A, while on the contrary, significantly less COL 1 was observed in group D than all 3 other groups. But still no significant difference was detected in distribution of COL 3 (Fig. 8F and G). Generally, as the elongation of intervention period, SaB-CPDA hydrogel showed superior anti-fibrosis effect and significantly reduce the deposition of collagen fibers (COL 1 especially) around the capsule of shoulder joint.

In addition, at week 9, all rats were euthanized and a part of the specimens were used to collect the glenohumeral joint synovium/capsule tissue for molecular biology analysis by performing western blotting and ELISA. The western blotting results suggested that the administration of SaB-CPDA could inhibit the expression of Fibronectin, COL 3, COL 1 and attenuate the pathologic fibrosis in vivo (Fig. 9A). And the secretion of tissue remodeling cytokines (TGF-β1, PDGF and CTGF) were also inhibited (Fig. 9B). Results of IHC showed decreased levels of inflammatory cytokines and chemokines (IL-1β, IL-6 and TNF-α) in shoulder joint after SaB-CPDA intervention, which echoed the results of western blotting and ELISA (Fig. 9C–F). Generally, the SaB-CPDA was associated with considerable anti-fibrosis and anti-inflammation ability in vivo (see Fig. 10).

In the current study, SaB-CPDA with excellent anti-oxidation ability and drug slow-release characteristics was developed to exert multiple functions for the treatment of FS, which included pathologic fibrosis and inflammation. SaB-CPDA boasts robust mechanical strength and impressive antibacterial and antioxidative capabilities, rendering it suitable for intra-articular injection. Water-soluble SaB is encapsulated within the CPDA hydrogel, facilitating gradual release over time. After a nine-week treatment period, our model rats exhibited recovery from FS, as evidenced by improvements in stride length and ROM parameters. Histological analysis provided compelling evidence for the effectiveness of SaB-CPDA in inhibiting pathological fibrosis. In addition to assessing the in vivo anti-fibrotic effects of drug-loaded hydrogels, we conducted further investigations at the cellular level to elucidate SaB's mechanisms of action. SaB not only directly inhibited the NFκB/IL-6 inflammatory pathway in synovial fibroblasts but also indirectly attenuated inflammation by inducing the polarization of macrophages towards the M2 phenotype. Both of these actions resulted in decreased expression of IL-6 and ECM proteins. Furthermore, SaB effectively inhibited ferroptosis in SFs. These results collectively suggest that the multifunctional SaB-CPDA platform holds promise as an innovative approach for the treatment of FS.

In material design, we employ CSMA to link PBA as the primary component, and the aldehyde group on OD-DA reacts with the Schiff
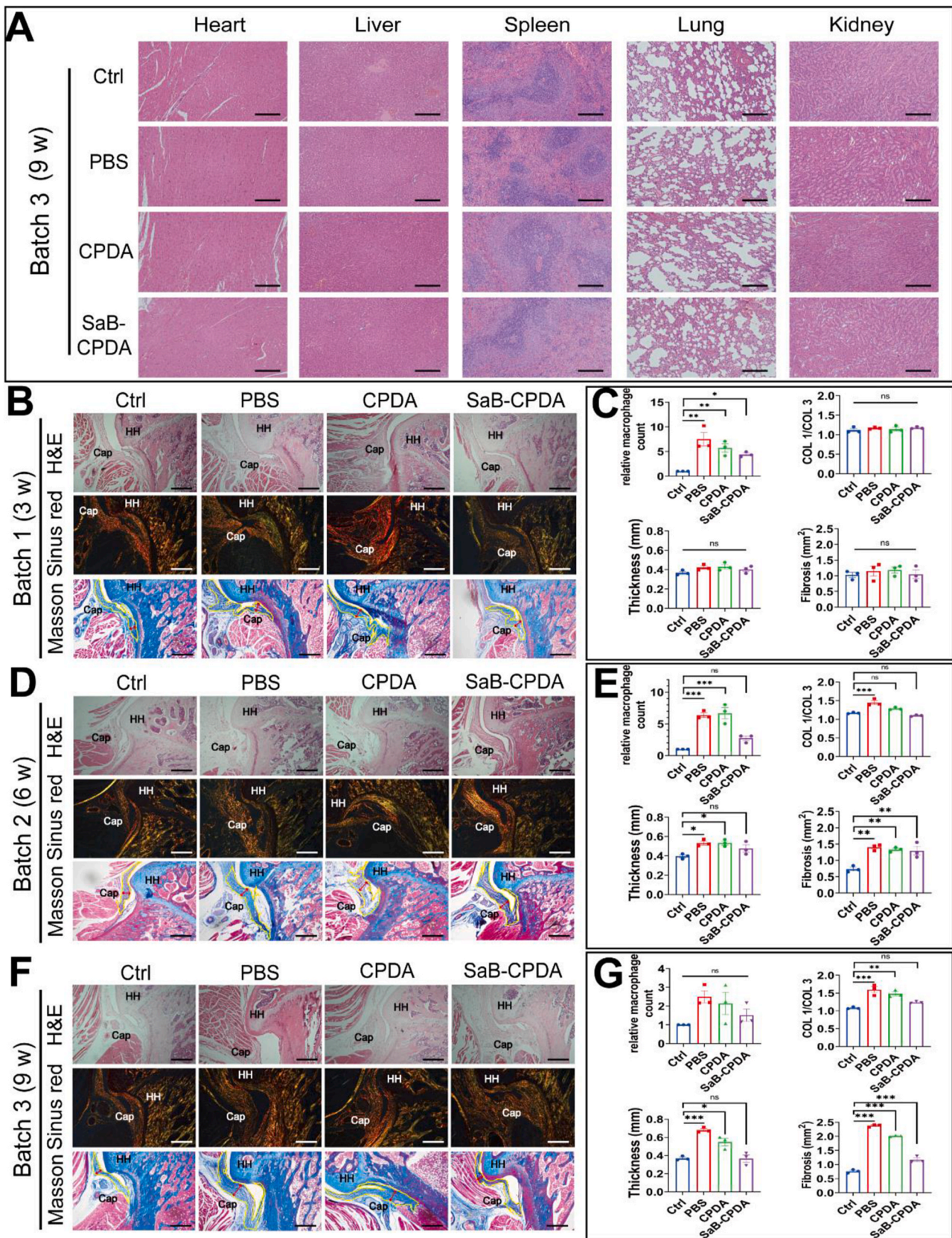
Fig. 8. Assessment of safety and anti-fibrotic ability of SaB-CPDA in vivo. A) H&E staining of slices of major internal organs derived from animals in different groups. Scale bar: 200 μm. HE staining, Masson's trichrome staining and Sirus red staining of shoulder joint slices were used for assessment of pathological fibrosis. All slices were obtained from animals underwent intervention for 3 weeks (B, C), 6 weeks (D, E) and 9 weeks (F, G) in different groups. Scale bar: 200 μm *P < 0.05; **P < 0.01; ***P < 0.001.
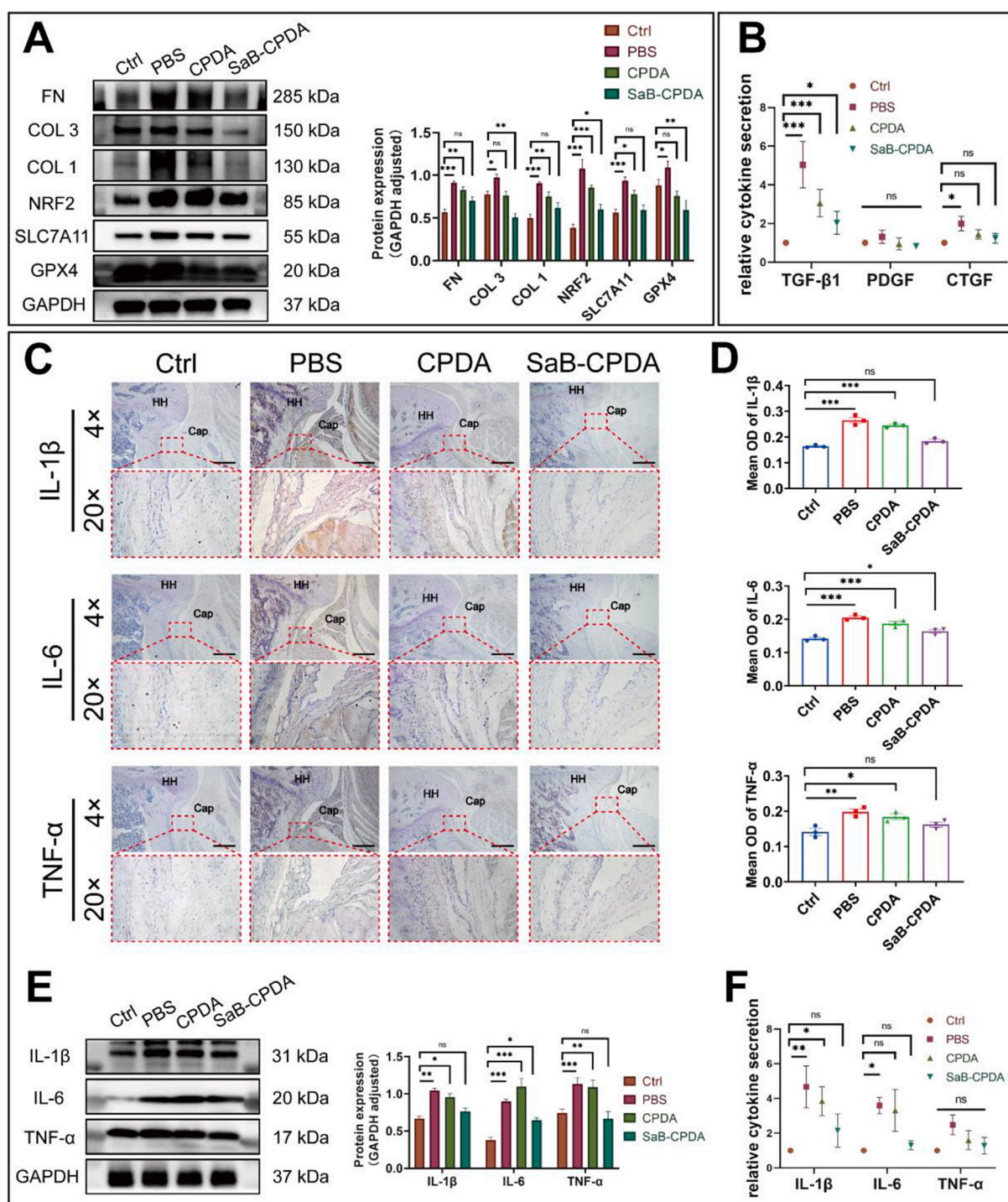
Fig. 9. Assessment of anti-fibrotic, anti-ferroptosis and anti-inflammation ability of SaB-CPDA in vivo. At week 9, all rats were euthanized for further experiments. A) Western blotting results derived from the synovium/capsule tissue of rats showed that the administration of SaB-CPDA could attenuate the pathologic fibrosis and ferroptosis process in vivo. B) And the secretion of tissue remodeling cytokines (TGF-β1, PDGF and CTGF) were also inhibited. C, D) IHC was also used for assessment of the levels of inflammatory cytokines and chemokines in shoulder joint. All slices were obtained from animals underwent intervention for 9 weeks in different groups. Scale bar: 200 μm. E, F) Western blotting and ELISA results both suggested that both the injection of SaB-CPDA in rat shoulder could counteract the inflammatory response in synovial/capsule tissue. *P < 0.05; **P < 0.01; ***P < 0.001.

base, forming the initial network. Upon UV irradiation, the double bond on the long chain of methacryloyl chitosan establishes the secondary network. Additionally, phenylboric acid and o-diphenol can create a boric acid ester bond. Key considerations for this design include pH response, glucose response, antibacterial and antioxidative effect. Firstly, inflammatory conditions lead to a decrease in the pH at the damaged site. The reversible Schiff base reaction under acidic conditions

opens the hydrogel network, enhancing drug release. Secondly, The PBA group on PPB can form a dynamic phenylborate bond with the catechol group on OD-DA. In the presence of glucose, competitive binding occurs between glucose and phenylboric acid. This leads to the dissociation of the coordination structure between phenylboric acid and catechol, opening the hydrogel network and increasing drug release. Finally, Chitosan, acting as a puncturing belt, disrupts the bacterial cell
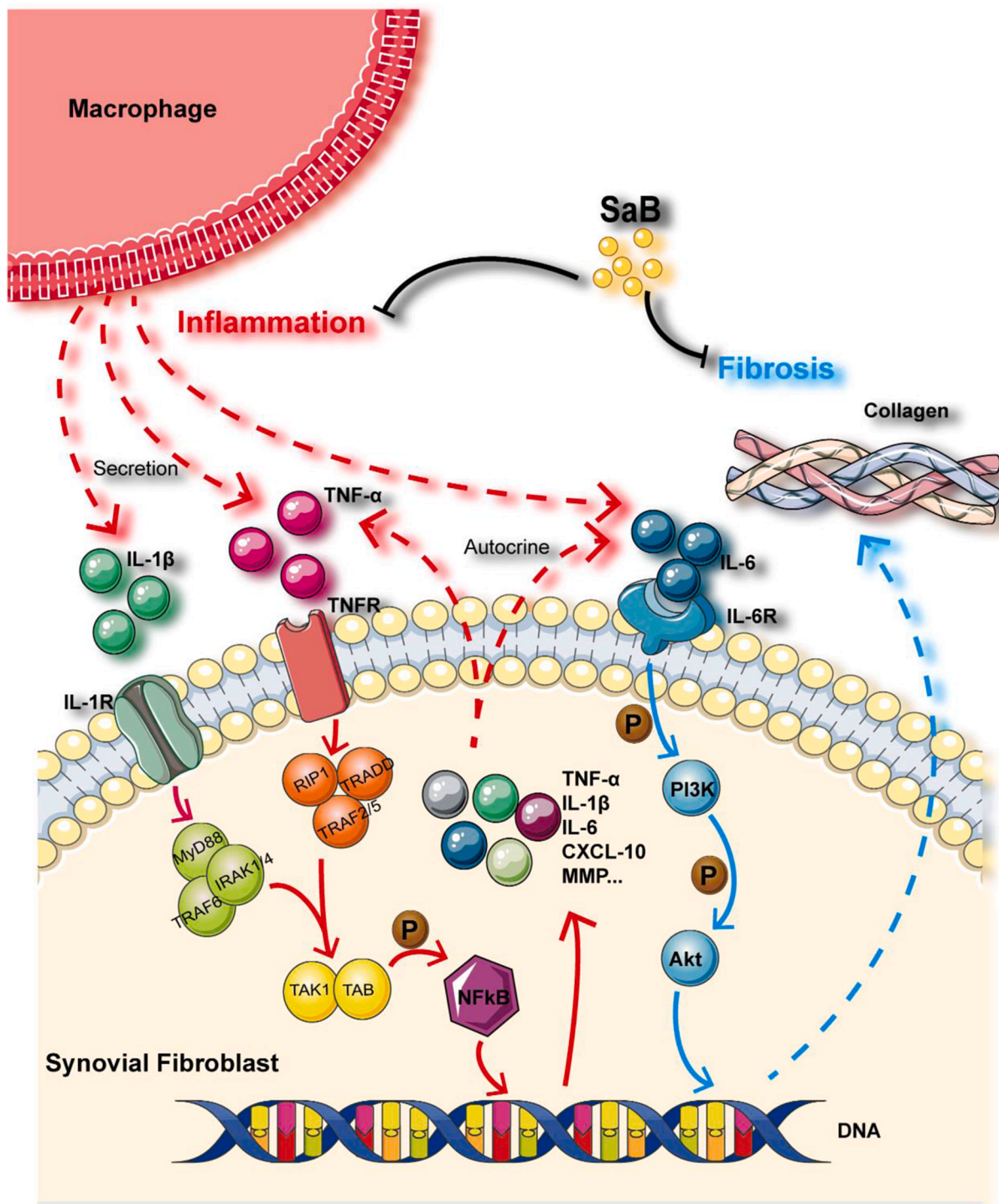
Fig. 10. SaB attenuates pathologic fibrosis in FS through both inflammatory and non-inflammatory pathways.

membrane while the o-diphenol group, primarily composed of dopamine, exhibits antioxidant properties [33,34,44]. To validate the design's reliability, we conducted a series of animal experiments. Following successful modeling in rats, we locally injected the drug-loaded hydrogel into the shoulder joint and observed its therapeutic effects. Stride length and ROM assessments generally revealed superior functional recovery in the SaB-CPDA group compared to the PBS and CPDA groups. Further histological examinations, including HE, Masson, and Sirius red staining, demonstrated that the SaB-CPDA group exhibited a significantly superior anti-fibrosis effect. These findings suggest that SaB-CPDA holds considerable clinical promise as a

treatment method for frozen shoulder.

Previous research has established SaB's anti-fibrotic efficacy in a range of fibrotic conditions, such as renal fibrosis, pulmonary fibrosis, cirrhosis, systemic sclerosis, and hyperplastic scars [25,27,45–47]. However, there is no prior evidence of SaB's application in FS treatment, except for our own research. Previously, we have demonstrated that SaB's anti-fibrosis effect is partially attributed to the inhibition of the CD36/PI3K-Akt pathway. Moreover, SaB induces a notably greater down-regulation of fibrosis-related proteins compared to CD36 knockdown alone. Additionally, the expression of inflammatory cytokines in synovial fibroblasts significantly decreased following SaB intervention

[28]. And there is evidence suggesting that IL-6 activates fibrotic signals via the PI3K/Akt pathway [22]. Based on the RNA-seq results, it is plausible to speculate that SaB down-regulates the expression of fibroproteins by suppressing the inflammatory pathway. Subsequent verification suggested that SaB exerts its anti-fibrotic effect by directly inhibiting the NFκB/IL-6 pathway in synovial fibroblasts, while also indirectly influencing the inflammatory response through macrophage polarization regulation. Besides, SaB inhibits the occurrence of ferroptosis in fibroblasts. However, the relationship between ferroptosis and fibrosis is controversial and requires further exploration. Consequently, these findings indicate that inflammation and fibrosis in FS are not entirely independent processes but rather intersecting networks. Interventions targeting inflammation or pathological fibrosis in FS may yield therapeutic benefits. SaB, with its potential in both inflammatory and non-inflammatory pathways, emerges as a promising therapeutic candidate for FS.

In fact, upon reviewing clinical guidelines and recommended therapeutic methods reported in the literature, we found that there is no widely recognized specific treatment for FS, especially those based on pathogenesis or targeting key molecules [2,5,6]. While intra-articular injection of glucocorticoid may be the most commonly used and effective treatment, its mid-term effectiveness is not satisfactory, let alone its long-term effects [7]. Therefore, we have preliminarily confirmed the anti-fibrotic effect of SaB both in vitro and in vivo [28] and have developed an injectable, drug-loaded, sustained-release hydrogel to address the limitations of its systemic use. Subsequently, a series of in vitro and in vivo experiments were conducted to assess its safety and efficacy, with the aim of providing insights for clinical practice. Additionally, building upon the injectable hydrogel for the shoulder joint, we hope to develop a convenient, non-invasive, safe, and efficient transdermal hydrogel patch for anti-fibrosis treatment. In the future, we believe that non-invasive treatments have the potential to replace the current recommended methods, such as oral nonsteroidal anti-inflammatory drugs, physiotherapy, and intra-articular injections, becoming the real gospel for FS patients.

There are, inevitably, certain limitations in this study. Firstly, while in vivo fluorescence imaging was used to assess SaB-CPDA's residence time in the capsule over seven days, it is important to note that detailed blood drug concentration data were not collected due to the absence of pharmacokinetic analysis. Secondly, although SaB has been shown to inhibit the activation of NFκB, further research is required to determine whether it plays this role directly or indirectly. Lastly, the synovium fibroblasts utilized in this study were obtained from patients with idiopathic FS, which implies that caution should be exercised when extrapolating these findings to FS of other types.

4. Conclusion

In conclusion, a novel, superior, antioxidant and antibacterial hydrogel was designed and synthesized for intra-articular delivery of SaB to deal with FS. SaB-CPDA was demonstrated to exhibit excellent therapeutic effect against FS both in vitro and in vivo. Furthermore, SaB attenuates FS development by inhibiting the inflammatory pathway. The anti-fibrotic effects of the SaB-loaded hydrogel represent a promising approach for treating FS and deserve further investigation in future research.

Ethics approval and consent to participate

The current study was approved by the Ethics Committee of the Sun Yat-sen Memorial Hospital of Sun Yat-sen University, Guangzhou, China (permit no: SYSKY-2023-872-01). Full informed consent was obtained from all patients.

CRediT authorship contribution statement

Yan Yan: Conceptualization, Methodology, Investigation, Writing – original draft. **Xinhao Li:** Methodology, Visualization. **Chen Chen:** Methodology, Formal analysis, Resources. **Dedong Cui:** Formal analysis, Software. **Zhuo Wang:** Methodology. **Ming Li:** Writing – original draft. **Yi Long:** Investigation, Data curation. **Jinming Zhang:** Visualization. **Cheng Li:** Project administration, Data curation. **Zhiling Wang:** Resources. **Chuanhai Zhou:** Writing – original draft. **Zeyu Yao:** Methodology. **Dan Wang:** Supervision. **Jingyi Hou:** Funding acquisition. **Rui Yang:** Supervision, Funding acquisition.

Declaration of competing interest

The authors declare that they have no known competing financial interests or personal relationships that could have appeared to influence the work reported in this paper.

Acknowledgements

Appendix A. Supplementary data

Supplementary data to this article can be found online at https://doi.org/10.1016/j.bioactmat.2024.06.009.

References

[1] A.S. Neviaser, R.J. Neviaser, Adhesive capsulitis of the shoulder, J. Am. Acad. Orthop. Surg. 19 (2011) 536–542.

[2] N.L. Millar, A. Meakins, F. Struyf, et al., Frozen shoulder, Nat. Rev. Dis. Prim. 8 (2022) 59.

[3] N. Shah, M. Lewis, Shoulder adhesive capsulitis: systematic review of randomised trials using multiple corticosteroid injections, Br. J. Gen. Pract. 57 (2007) 662–667.

[4] L.H. Redler, E.R. Dennis, Treatment of adhesive capsulitis of the shoulder, J. Am. Acad. Orthop. Surg. 27 (2019) e544–e554.

[5] J. Ramirez, Adhesive capsulitis: diagnosis and management, Am. Fam. Physician 99 (2019) 297–300.

[6] C.H. Cho, K.C. Bae, D.H. Kim, Treatment strategy for frozen shoulder, Clin. Orthop. Surg. 11 (2019) 249–257.

[7] D. Challoumas, M. Biddle, M. McLean, N.L. Millar, Comparison of treatments for frozen shoulder: a systematic review and meta-analysis, JAMA Netw. Open 3 (2020) e2029581.

[8] B. Shaffer, J.E. Tibone, R.K. Kerlan, Frozen shoulder. A long-term follow-up, J Bone Joint Surg Am 74 (1992) 738–746.

[9] T.D. Bunker, J. Reilly, K.S. Baird, D.L. Hamblen, Expression of growth factors, cytokines and matrix metalloproteinases in frozen shoulder, Journal of Bone and Joint Surgery - Series B 82 (2000) 768–773.

[10] G.C.R. Hand, N.A. Athanasou, T. Matthews, A.J. Carr, The pathology of frozen shoulder, J. Bone Jt. Surg. Br. Vol. 89-B (2007) 928–932.

[11] Y. Hagiwara, A. Ando, Y. Onoda, et al., Coexistence of fibrotic and chondrogenic process in the capsule of idiopathic frozen shoulders, Osteoarthritis Cartilage 20 (2012) 241–249.

[12] S.A. Rodeo, J.A. Hannafin, J. Tom, R.F. Warren, T.L. Wickiewicz, Immunolocalization of cytokines and their receptors in adhesive capsulitis of the shoulder, J. Orthop. Res. 15 (1997) 427–436.

[13] B. Kabbabe, S. Ramkumar, M. Richardson, Cytogenetic analysis of the pathology of frozen shoulder, Int. J. Shoulder Surg. 4 (2010) 75–78.

[14] A.M.T. Lubis, V.K. Lubis, Matrix metalloproteinase, tissue inhibitor of metalloproteinase and transforming growth factor-beta 1 in frozen shoulder, and their changes as response to intensive stretching and supervised neglect exercise, J. Orthop. Sci. 18 (2013) 519–527.

[15] M. Akbar, M. McLean, E. Garcia-Melchor, et al., Fibroblast activation and inflammation in frozen shoulder, PLoS One 14 (2019).

[16] S.G. Dakin, A. Rangan, F. Martinez, et al., Tissue inflammation signatures point towards resolution in adhesive capsulitis, Rheumatology 58 (2019) 1109–1111.

[17] C. Guyot, S. Lepreux, C. Combe, et al., Hepatic fibrosis and cirrhosis: the (myo) fibroblastic cell subpopulations involved, Int. J. Biochem. Cell Biol. 38 (2006) 135–151.

[18] Y.B.Y. Sun, X. Qu, G. Caruana, J. Li, The origin of renal fibroblasts/myofibroblasts and the signals that trigger fibrosis, Differentiation 92 (2016) 102–107.

[19] K. Tsoyi, S.G. Chu, N.G. Patino-Jaramillo, et al., Syndecan-2 attenuates radiation-induced pulmonary fibrosis and inhibits fibroblast activation by regulating PI3K/Akt/ROCK pathway via CD148, Am. J. Respir. Cell Mol. Biol. 58 (2018) 208–215.

[20] R. Yang, H. Deng, J. Hou, et al., Investigation of salmon calcitonin in regulating fibrosis-related molecule production and cell-substrate adhesion in frozen shoulder synovial/capsular fibroblasts, J. Orthop. Res. 38 (2020) 1375–1385.

[21] M. Akbar, L.A.N. Crowe, M. McLean, et al., Translational targeting of inflammation and fibrosis in frozen shoulder: molecular dissection of the T cell/IL-17A axis, Proc. Natl. Acad. Sci. U. S. A 118 (2021).

[22] R. Yang, Y. Tang, J. Hou, et al., Fibrosis in frozen shoulder: activation of IL-6 through PI3K-Akt signaling pathway in synovial fibroblast, Mol. Immunol. 150 (2022) 29–38.

[23] Z. Xiao, W. Liu, Y.P. Mu, et al., Pharmacological effects of salvianolic acid B against oxidative damage, Front. Pharmacol. 11 (2020) 572373.

[24] X.M. Tao, D. Li, C. Zhang, et al., Salvianolic acid B protects against acute and chronic liver injury by inhibiting Smad2C/L phosphorylation, Exp. Ther. Med. 21 (2021) 341.

[25] T. Zhang, M. Liu, Y. Gao, et al., Salvianolic acid B inhalation solution enhances antifibrotic and anticoagulant effects in a rat model of pulmonary fibrosis, Biomed. Pharmacother. 138 (2021) 111475.

[26] C. Wu, W. Chen, H. Ding, et al., Salvianolic acid B exerts anti-liver fibrosis effects via inhibition of MAPK-mediated phospho-Smad2/3 at linker regions in vivo and in vitro, Life Sci. 239 (2019) 116881.

[27] M.F. Griffin, M.R. Borrelli, J.T. Garcia, et al., JUN promotes hypertrophic skin scarring via CD36 in preclinical in vitro and in vivo models, Sci. Transl. Med. 13 (2021) eabb3312.

[28] Y. Yan, M. Zhou, K. Meng, et al., Salvianolic acid B attenuates inflammation and prevent pathologic fibrosis by inhibiting CD36-mediated activation of the PI3K-Akt signaling pathway in frozen shoulder, Front. Pharmacol. 14 (2023) 1230174.

[29] Z. Sun, C. Song, C. Wang, Y. Hu, J. Wu, Hydrogel-based controlled drug delivery for cancer treatment: a review, Mol. Pharm. 17 (2020) 373–391.

[30] L. Hu, J. Zhou, Z. He, et al., In situ-formed fibrin hydrogel scaffold loaded with human umbilical cord mesenchymal stem cells promotes skin wound healing, Cell Transplant. 32 (2023) 9636897231156215.

[31] A. Abbadessa, M.M. Blokzijl, V.H. Mouser, et al., A thermo-responsive and photo-polymerizable chondroitin sulfate-based hydrogel for 3D printing applications, Carbohydr. Polym. 149 (2016) 163–174.

[32] Y. Liang, Z. Li, Y. Huang, R. Yu, B. Guo, Dual-dynamic-bond cross-linked antibacterial adhesive hydrogel sealants with on-demand removability for post-wound-closure and infected wound healing, ACS Nano 15 (2021) 7078–7093.

[33] Y. Liang, M. Li, Y. Yang, L. Qiao, H. Xu, B. Guo, pH/glucose dual responsive metformin release hydrogel dressings with adhesion and self-healing via dual-

dynamic bonding for athletic diabetic foot wound healing, ACS Nano 16 (2022) 3194–3207.

[34] Y. Huang, L. Mu, X. Zhao, Y. Han, B. Guo, Bacterial growth-induced tobramycin smart release self-healing hydrogel for Pseudomonas aeruginosa-infected burn wound healing, ACS Nano 16 (2022) 13022–13036.

[35] S.M. Okajima, M.B. Cubria, S.J. Mortensen, et al., Rat model of adhesive capsulitis of the shoulder, J. Vis. Exp. (2018) e58335.

[36] K.I. Kim, Y.S. Lee, J.Y. Kim, S.W. Chung, Effect of diabetes and corticosteroid injection on glenohumeral joint capsule in a rat stiffness model, J. Shoulder Elbow Surg. 30 (2021) 2814–2823.

[37] D.H. Kim, K.H. Lee, Y.M. Lho, et al., Characterization of a frozen shoulder model using immobilization in rats, J. Orthop. Surg. Res. 11 (2016) 160.

[38] S. Oki, H. Shirasawa, M. Yoda, et al., Generation and characterization of a novel shoulder contracture mouse model, J. Orthop. Res. 33 (2015) 1732–1738.

[39] A. Chainani, A. Matson, M. Chainani, et al., Contracture and transient receptor potential channel upregulation in the anterior glenohumeral joint capsule of patients with end-stage osteoarthritis, J. Shoulder Elbow Surg. 29 (2020) e253–e268.

[40] P. Li, Z. Hao, J. Wu, et al., Comparative proteomic analysis of polarized human THP-1 and mouse RAW264.7 macrophages, Front. Immunol. 12 (2021) 700009.

[41] H. Yu, L. Lin, Z. Zhang, H. Zhang, H. Hu, Targeting NF-κB pathway for the therapy of diseases: mechanism and clinical study, Signal Transduct. Targeted Ther. 5 (2020) 209.

[42] M. Arra, G. Swarnkar, K. Ke, et al., LDHA-mediated ROS generation in chondrocytes is a potential therapeutic target for osteoarthritis, Nat. Commun. 11 (2020) 3427.

[43] H. Zhang, H. Xiong, W. Ahmed, et al., Reactive oxygen species-responsive and scavenging polyurethane nanoparticles for treatment of osteoarthritis in vivo, Chem. Eng. J. 409 (2021) 128147.

[44] L. Qiao, Y. Liang, J. Chen, et al., Antibacterial conductive self-healing hydrogel wound dressing with dual dynamic bonds promotes infected wound healing, Bioact. Mater. 30 (2023) 129–141.

[45] Y. He, R. Lu, J. Wu, et al., Salvianolic acid B attenuates epithelial-mesenchymal transition in renal fibrosis rats through activating Sirt1-mediated autophagy, Biomed. Pharmacother. 128 (2020) 110241.

[46] H.Y. Gao, G.Y. Li, M.M. Lou, X.Y. Li, X.Y. Wei, J.H. Wang, Hepatoprotective effect of matrine salvianolic acid B salt on carbon tetrachloride-induced hepatic fibrosis, J. Inflamm. 9 (2012) 16.

[47] Q. Liu, J. Lu, J. Lin, et al., Salvianolic acid B attenuates experimental skin fibrosis of systemic sclerosis, Biomed. Pharmacother. 110 (2019) 546–553.